

Geosphere

Fault interaction and along-strike variation in throw in the Pajarito fault system, Rio Grande rift, New Mexico

Claudia J. Lewis, Jamie N. Gardner, Emily S. Schultz-Fellenz, Alexis Lavine, Steven L. Reneau and Susan Olig

Geosphere 2009;5;252-269
doi: 10.1130/GES00198.1

Email alerting services click www.gsapubs.org/cgi/alerts to receive free e-mail alerts when new articles cite this article

Subscribe click www.gsapubs.org/subscriptions/ to subscribe to Geosphere

Permission request click <http://www.geosociety.org/pubs/copyrt.htm#gsa> to contact GSA

Copyright not claimed on content prepared wholly by U.S. government employees within scope of their employment. Individual scientists are hereby granted permission, without fees or further requests to GSA, to use a single figure, a single table, and/or a brief paragraph of text in subsequent works and to make unlimited copies of items in GSA's journals for noncommercial use in classrooms to further education and science. This file may not be posted to any Web site, but authors may post the abstracts only of their articles on their own or their organization's Web site providing the posting includes a reference to the article's full citation. GSA provides this and other forums for the presentation of diverse opinions and positions by scientists worldwide, regardless of their race, citizenship, gender, religion, or political viewpoint. Opinions presented in this publication do not reflect official positions of the Society.

Notes

Fault interaction and along-strike variation in throw in the Pajarito fault system, Rio Grande rift, New Mexico

Claudia J. Lewis

Jamie N. Gardner*

Emily S. Schultz-Fellenz

Alexis Lavine[†]

Steven L. Reneau

Los Alamos National Laboratory, EES-16, MS D452, Los Alamos, New Mexico 87545, USA

Susan Olig

URS Corporation, 1333 Broadway, Suite 800, Oakland, California 94612, USA

ABSTRACT

The seismically active Pajarito fault system (PFS) of northern New Mexico, United States, is a complex zone of deformation made up of many laterally discontinuous faults and associated folds and fractures that interact in ways that have important implications for seismic hazards. Mapping and drilling projects in the PFS provide new insights into the structural geometry and paleoseismic history of the fault system. A 1.25 Ma old datum (the Bandelier Tuff) and high-resolution digital elevation data allow construction of throw-length profiles along the entire length of the PFS, revealing primary geometric features previously unrecognized. The fault system as a whole consists of numerous closely spaced overlapping sections ~8–14 km long. Slip maxima in some cases occur near the centers of these sections, and in others they are shifted toward one end. Along-strike asymmetrical throw profiles and throw deficits indicate fault branching, merging, and strain transfer. This pattern results from processes of fault linkage and conservation of strain on diverse structures of a large fault system. New mapping reveals that the northern end of the Pajarito fault terminates in a wide zone of extensional monoclines and discontinuous, small-displacement faults, and interacts with nearby antithetic faults. New paleoseismic data from a normal fault splay, interpreted in light of previous paleoseismic work, argue

for three Holocene surface-rupturing earthquakes; one ca. 1.4 thousand calendar years ago (1.4 cal ka) on the Pajarito fault, a second 6.5–5.2 ka ago on the Pajarito fault that is consistent with an event 6.5–4.2 ka ago on the Guaje Mountain fault, and a third ca. 9 ka ago on both the Pajarito and the Rendija Canyon faults. This paleoseismic event chronology demonstrates that the Pajarito fault often ruptures alone, but sometimes ruptures either with the Rendija Canyon or the Guaje Mountain fault. When this occurs, the resultant seismic moment and therefore the earthquake magnitude are larger than when the main Pajarito fault ruptures alone. Evidence for fault interaction, and the presence of prominent bends in the Pajarito fault system, imply structural control of paleoseismicity and neoseismicity and suggest the potential for stress concentrations and earthquake triggering in complex linking fault systems.

INTRODUCTION

The Pajarito fault system (PFS; Fig. 1), New Mexico, United States, is tectonically active, comprising the active bounding faults of the Española basin of the Rio Grande rift, and is the subject of ongoing paleoseismic investigations. Paleoseismic data from the PFS demonstrate at least two, and possibly three, surface-rupturing events in Holocene time (e.g., Wong et al., 1995; Kelson et al., 1996; Reneau et al., 2002; Gardner et al., 2003; McCalpin, 2005), but all of them on

different fault strands. Despite the importance of understanding the geometry of the fault system and potential linkage among faults for purposes of seismic hazard analysis, a robust kinematic model of the fault system is lacking.

Most normal fault systems, including the PFS, are characterized by significant geometric irregularity, including lateral variation in displacement, strike and dip, and complexity of faulting. The PFS is an en echelon array of faults and folds. En echelon fault arrays evolve into through-going structures by linkage of overlapping segments either by propagation of fault tips or by formation of new connecting faults (e.g., Peacock and Sanderson, 1994; Trudgill and Cartwright, 1994; Crider, 2001). Forced folds may develop as fault tips propagate upward or laterally, forming monoclines or faulted monoclines as deformation progresses (e.g., Withjack et al., 1990; Hardy and McClay, 1999; Withjack and Callaway, 2000; Willsey et al., 2002). Processes of fault linkage and propagation can therefore result in complex fault geometry. This has been shown in analog and numerical models and field examples of fault systems across a range of scales.

Unraveling the kinematics of a complex system like the PFS to test hypotheses of fault linkage and propagation requires time-stratigraphic markers to determine displacement along the length of the fault system and to define fault activity temporally. In the Jemez Mountains of northern New Mexico, a distinctive Pleistocene geologic unit, the Bandelier Tuff, provides exceptional stratigraphic markers with which to

*Present address: Gardner Geoscience, 14170 Highway 4, Jemez Springs, New Mexico 87025, USA.

[†]Present address: Geomatrix Consultants, Inc., 2101 Webster St., Oakland, California 94612, USA.

measure structural displacements (Fig. 2). The PFS cuts the Bandelier Tuff nearly end to end along its 50 km length. In this paper we use the 1.25 Ma old (Phillips, 2004) Tshirege Member of the Bandelier Tuff as a datum to construct a composite throw profile for the PFS. Nevertheless, throw on Bandelier Tuff integrates fault ruptures that have occurred over the past 1.25 Ma. To understand patterns of fault interaction requires paleoseismic data that demonstrate

which fault strands rupture, and when. Combining new paleoseismic results and detailed mapping of fault deformation affecting the Bandelier Tuff, we propose a model of the fault system's geometry and Quaternary evolution that takes into account evidence for propagation and linkage of principal fault strands.

In addition to neotectonics, the results of this study have implications for investigations of normal fault systems of any age in any tec-

tonic setting. These results will be of interest to researchers who study tectonic geomorphology, in particular modelers of basin evolution and surface processes, hydrologists who model fluid flow in rift basins, and geophysicists who study extensional seismicity, crustal-scale structure, and the lithospheric evolution of rift systems.

GEOLOGIC SETTING

The study area is at the eastern edge of the Jemez Mountains at the intersection of the Rio Grande rift and the Jemez lineament (Fig. 1). The Rio Grande rift is a middle Tertiary–Quaternary system of asymmetric rift basins (e.g., Kelley, 1979) that extends from southern New Mexico to southern Wyoming. The study area is located in the Española basin, a half-graben bounded on the west by the PFS (Fig. 1), parts of which have been active since mid-Miocene time. Strata of the Miocene rift-filling Santa Fe Group dip gently to moderately westward toward the fault system.

Basaltic to rhyolitic volcanic activity accompanied formation of the Española basin. In the Jemez Mountains, volcanic activity started ca. 23 Ma ago at isolated basaltic centers (e.g., Gardner and Goff, 1984; WoldeGabriel et al., 2003). The culmination of the volcanic field's development occurred in Quaternary time with eruption of the Bandelier Tuff, resulting in deposition of 650 km³ (dense rock equivalent; Self et al., 1986) of rhyolitic ash flow tuffs in the Valles-Toledo caldera, which collapsed as a result of the eruption, and on the plateaus that now surround it (Fig. 1). Activity on the PFS continued after Bandelier Tuff deposition, resulting in the present fault deformation of the tuff.

PREVIOUS WORK

The PFS is a series of faults and fault zones that defines the active western and northwestern boundary of the Española basin (Griggs, 1964; Smith et al., 1970; Kelley, 1979; Boden, 1980; Golombek, 1981; Gardner and House, 1987). The Pajarito fault, namesake of the fault system, is the principal, crustal-scale normal fault at the basin boundary, but the Rendija Canyon, Guaje Mountain, Sawyer Canyon, and Puye faults all formed in response to the same regional stress system as the Pajarito fault, and are considered part of the PFS (Carter and Gardner, 1996) (Fig. 3). Components of the PFS are described in the following and were mapped by Gardner and House (1987), Goff et al. (1990), McCalpin (1997), Smith and Kuhle (1998), Gardner et al. (1999, 2001), Goff et al. (2001), Kempton and Kelley (2002), Lewis et al. (2002), Lynch et al. (2004), and Koning et al. (2005).

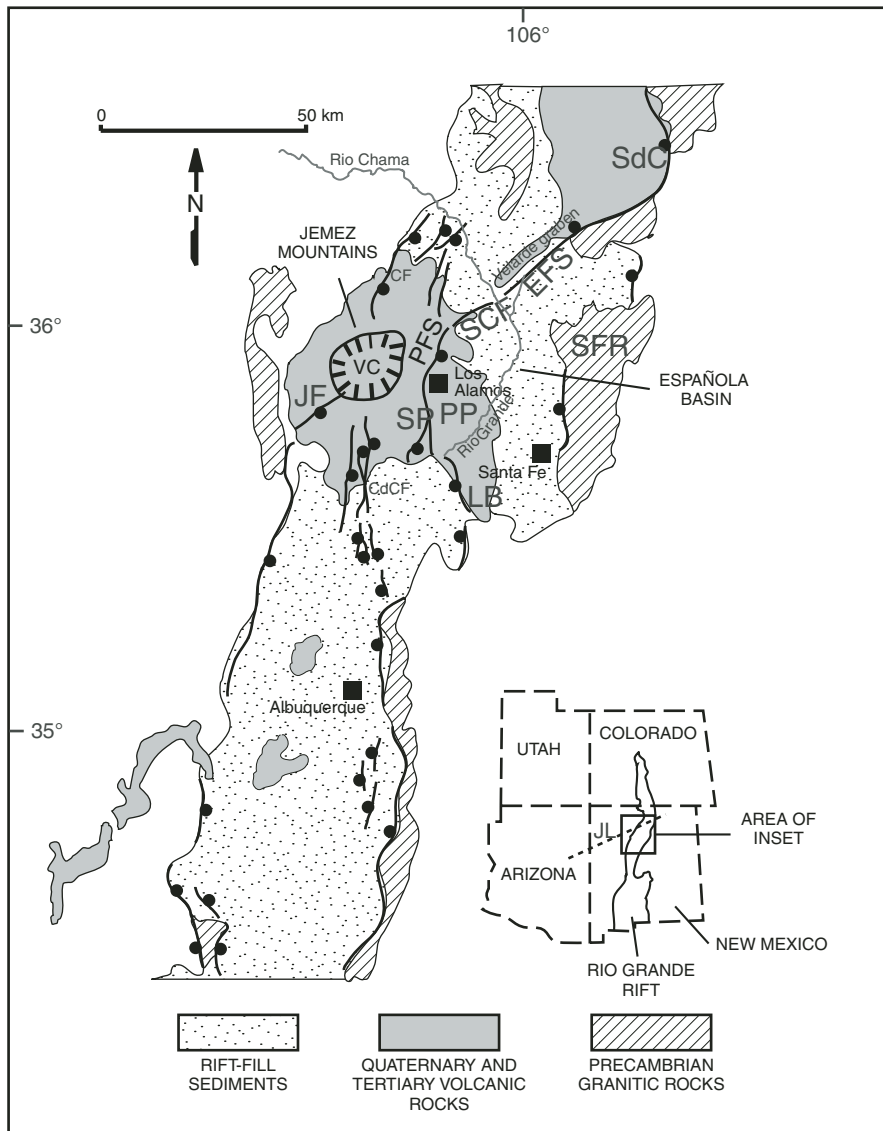


Figure 1. Map of the Rio Grande rift in northern New Mexico schematically showing location of the Pajarito fault system (PFS) with respect to other major fault systems (ball on downthrown side). Abbreviations: CF—Cañones fault zone; CdCF—Cañada de Cochiti fault zone; EFS—Embudo fault system; JF—Jemez fault zone; JL—Jemez lineament; LB—La Bajada fault; PP—Pajarito Plateau; SCF—Santa Clara fault (Koning et al., 2004); SdC—Sangre de Cristo fault; SFR—Santa Fe Range; SP—St. Peter's Dome; VC—Valles-Toledo caldera complex, the source of the Bandelier Tuff. Modified from Gardner and Goff (1984).

Pajarito Fault

The Pajarito fault (PF) strikes north to northeast through Bandelier National Monument and the city of Los Alamos (Figs. 1 and 3). The geometry of the fault varies appreciably along strike (e.g., McCalpin 1997, 2005; Gardner et al., 1999; this study). The PF is expressed at the surface as a large normal fault escarpment, a faulted monocline, and a zone of distributed deformation with significant down-to-the-east vertical displacement on the Tshirege Member of the Bandelier Tuff. Maximum throw on the PF occurs south of Frijoles Canyon, where it is expressed at the surface as two parallel down-to-the-east normal faults with ~180 m throw on Bandelier Tuff on the westernmost fault and ~90 m on the eastern fault (Fig. 3, site G; Gardner and House, 1987; Reneau, 2000).

The paleoseismic event chronology of the PF has been addressed by a series of studies (Wong et al., 1995, 2007; Olig et al., 1996; Reneau et al., 2002; McCalpin, 2005). Fourteen trenches excavated across strands of the PF (McCalpin, 2005) revealed details of the geometry of faulting, the style and timing of post-Bandelier deposition, and the paleoseismic event chronology. Four of these trenches (97–3, 97–4, 97–7, and 97–7A; Animation 1) displayed evidence of a middle to late Holocene “most recent” event. The most recent event identified in trenches 97–7 and 97–7a (located on the same fault several meters apart) is tightly delimited by radiocarbon dates of ca. 1.5 radiocarbon ka B.P., or 1.4 cal (calendar) ka ago (McCalpin, 2005). In trenches 97–3 and 97–4 (located on the same fault ~100 m apart but on a different strand than trenches 97–7 and 97–7a), the most recent event

is well defined at 6.5–5.2 cal ka ago (McCalpin, 2005). This is clearly not the event identified in trenches 97–7 and 97–7a.

Further trench exposures characterized the stratigraphy and structure of the east side of a graben at the base of the PF escarpment (Fig. 3, blue star), providing evidence for a minimum of six surface rupturing events in the past 1.25 Ma and demonstrating the recurring nature of surface faulting at the site (Reneau et al., 2002). The most recent event occurred more recently than 10.5 cal ka ago. If a prominent alignment of stones identified in the trench represents mass wasting during the most recent event, the event occurred between 8.6 and 5.5 cal ka ago, most likely closer to 8.6 cal ka ago. It is also possible that the stone line was formed not during a paleoseismic event on the PF, but during a paleoseismic event elsewhere in the fault system or the region.

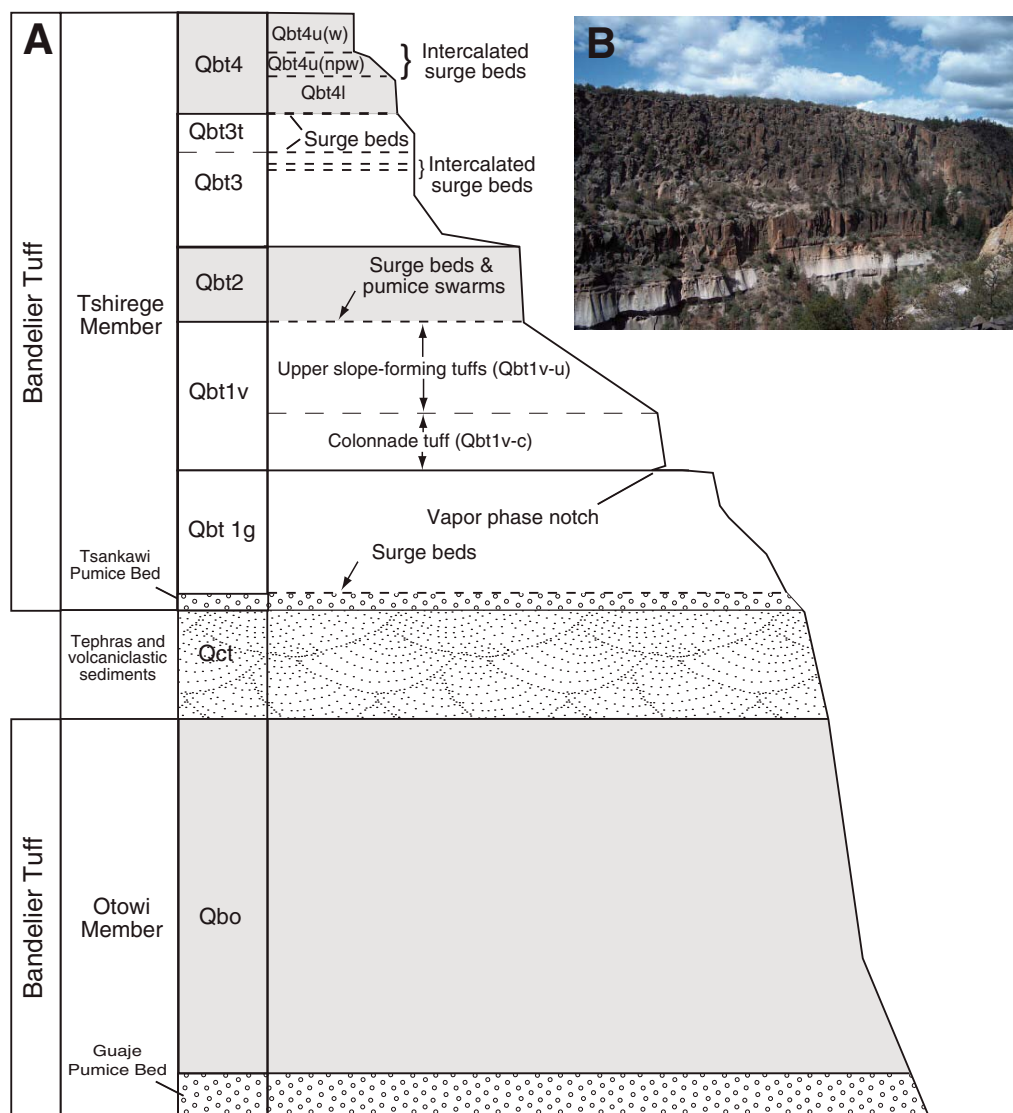


Figure 2. (A) Stratigraphy of the Bandelier Tuff for the area of detailed mapping (Broxton and Reneau, 1995; Lewis et al., 2002). Section is schematic; thickness of the Bandelier Tuff across the Pajarito Plateau varies by location. The most complete sections of Tshirege Member are located in the central part of the plateau in and near Los Alamos National Laboratory and Bandelier National Monument. (B) Photo of section of canyons of the Pajarito Plateau. Approximate thickness of Bandelier Tuff shown in the photo is 183 m.

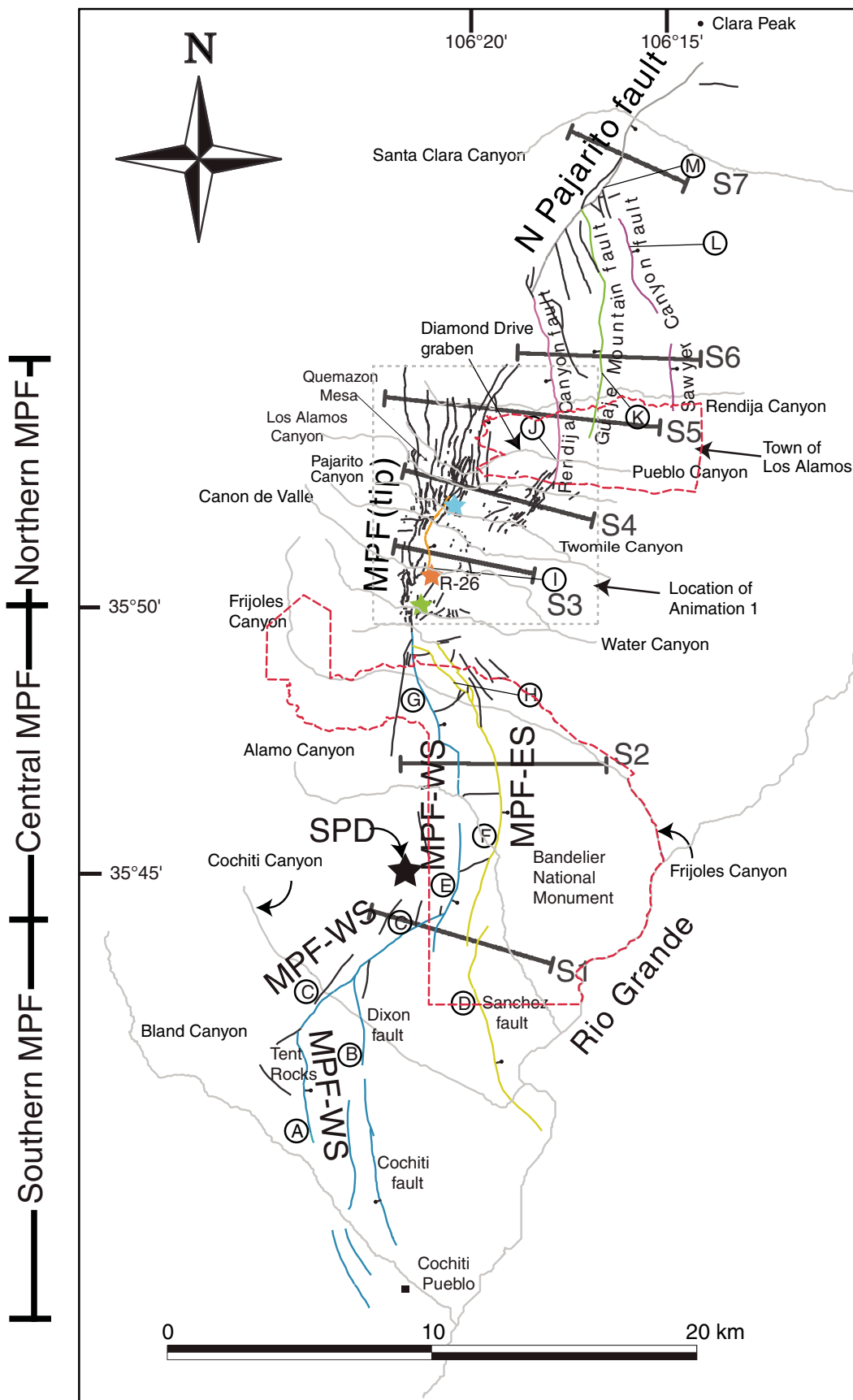
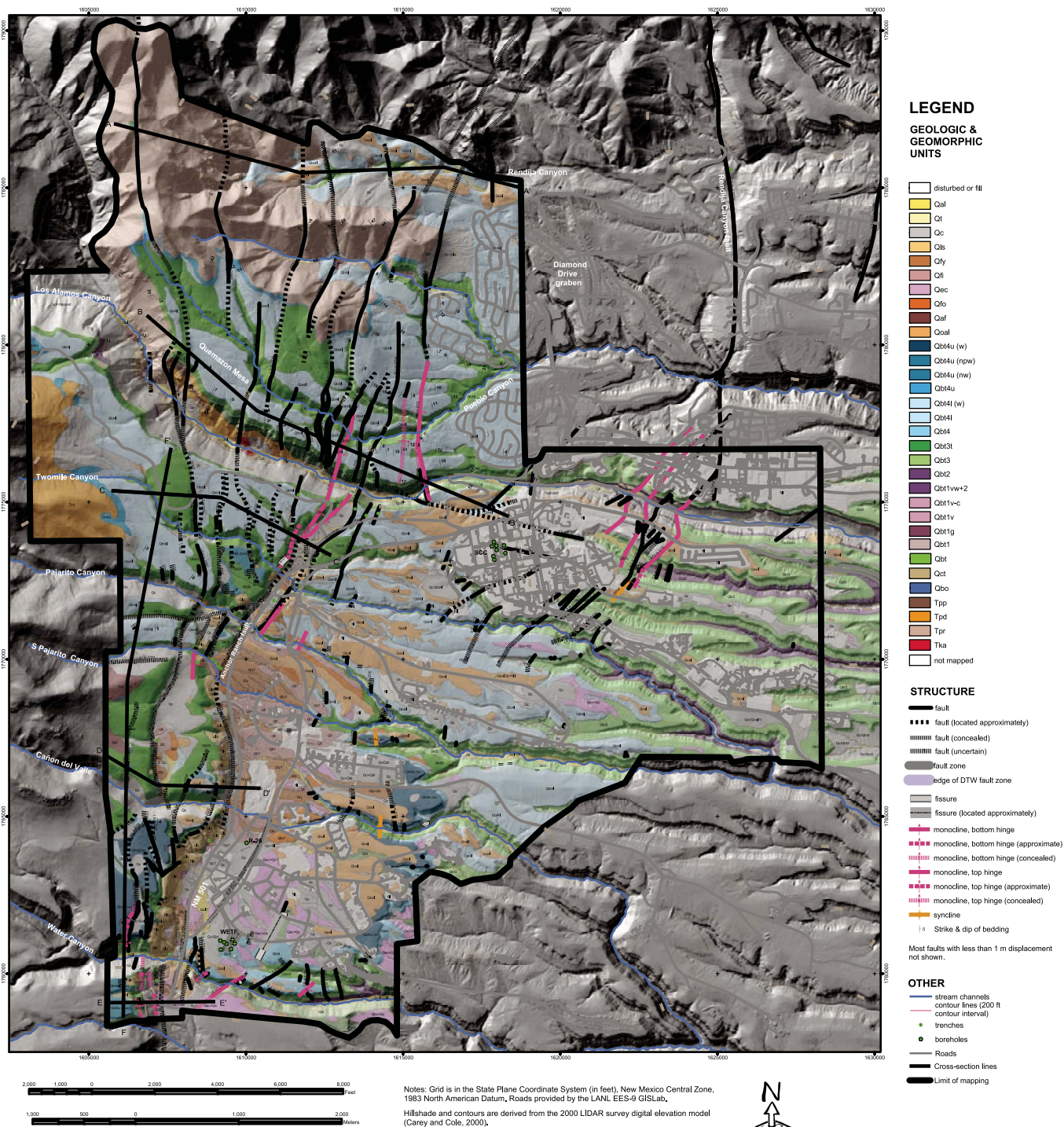


Figure 3. Map showing the 50-km-long Pajarito fault system. Thick gray lines (S1–S7) provide locations of cross sections shown in Figure 8. Circled letters A–M indicate portions of the fault system referenced in Figure 5. Green star shows location of borehole 2C (Gardner et al., 2001). Blue star indicates location of Reneau et al. (2002) trench. Orange star indicates location of well R-26 (Kleinfelder Inc., 2005). SPD—St. Peter’s Dome; MPF—main Pajarito fault (WS—west splay; ES—east splay). Colors of fault lines as in Figure 5.

Geologic map of the Pajarito fault system near Los Alamos, NM



Animation 1. Geologic map of the Pajarito fault system west of and within Los Alamos National Laboratory and the town of Los Alamos with embedded lithologic descriptions and photographs. To view the stratigraphic descriptions and photos embedded in the map, you will need Acrobat Adobe 8.0 or higher. If you are viewing the PDF of this paper or reading it offline, please visit <http://dx.doi.org/10.1130/GES00198.S1> or the full-text article at <http://geosphere.gsapubs.org> to view the animation.

Rendija Canyon Fault

The Rendija Canyon fault (RCF) is a dominantly down-to-the-west normal fault that, along with the down-to-the-east PF, bounds the Diamond Drive graben (Fig. 3; Gardner et al., 1999). The graben trends north and is beneath the western part of Los Alamos. The 14-km-long RCF is located ~3 km east of the PF (Gardner and House, 1987; Gardner et al., 1999). It exhibits as much as 40 m of post-Bandelier Tuff down-to-the-west displacement (Carter and Gardner, 1996; Olig et al., 1996). South of the town of Los Alamos, the RCF splays southwest into a zone of deformation ~1500 m wide with evidence for monoclinical folding and high-angle reverse faulting, as well as normal faulting in which northeast-striking normal faults generally have <3 m of normal throw, and monoclines and faulted monoclines accommodate <15 m of cumulative throw on Bandelier Tuff (e.g., Gardner et al., 1999). This zone of distributed deformation, including gentle northward tilts of structural blocks, forms part of the diffuse southern boundary of the Diamond Drive graben (Fig. 3). Net down-to-the-west displacement gradually decreases to the south as the zone of deformation broadens; faulting probably dies out just south of Twomile Canyon (Fig. 3), where net down-to-the-west throw is ~10 m on Bandelier Tuff.

Trench exposures across the southern termination of the RCF provided evidence of three or four surface ruptures since deposition of colluvium deposited before 140 ± 26 ka ago (Wong et al., 1995; Kelson et al., 1996). Charcoal samples from unfaulted strata yielded an average age of 8.1 ± 0.2 cal ka, whereas thermoluminescence analyses gave an average age of 23 ± 4 ka. These studies concluded that the most recent rupture occurred ca. 9 ka ago. Fluvial terrace deposits as young as 4.0–0.5 ka were not faulted (McDonald et al., 1996; Olig et al., 1996), indicating no paleoseismic event younger than ca. 9 ka ago.

Guaje Mountain Fault

The Guaje Mountain fault (GMF) is located ~2 km east of the subparallel RCF and ~5 km east of the PF (Fig. 3; Gardner and House, 1987; Gardner et al., 1999). It is somewhat shorter than the RCF and exhibits ~35 m of down-to-the-west throw (Carter and Gardner, 1996; Olig et al., 1996). The southern extent and amount of displacement of the GMF are not well characterized. The fault loses topographic expression between Rendija and Pueblo Canyons (Fig. 3; Gardner et al., 2003).

Trenches excavated across the GMF provide evidence for repeated late Quaternary surface ruptures, including a Holocene event (Gard-

ner et al., 2003). The most recent event on the GMF occurred in mid-Holocene time, ca. 6.5–4.2 cal ka ago. This event is tightly delimited in one trench, and evidence from other trenches is consistent with this timing (Gardner et al., 2003). Strata exposed in the trenches dated 3.8–0.3 cal ka ago are not faulted, indicating no paleoseismic event younger than 4.2 cal ka ago along the fault.

Embudo Fault System

The 65-km-long Embudo fault system (Fig. 1) forms the structural boundary between two actively subsiding asymmetric half-grabens, the east-tilted San Luis basin to the north and the west-tilted Española basin to the south. The 20-km-long northeastern segment has been dominated by left-lateral strike slip since the late Tertiary and shows evidence of late Quaternary left-oblique slip along discontinuous fault strands distributed over a width of several kilometers (e.g., Kelson et al., 2004). The 45-km-long southwestern section, termed the Santa Clara fault (Koning et al., 2004), shows ~500 m of normal displacement on middle Miocene basalts, ~40 m of normal displacement on an early Pleistocene terrace (Harrington and Aldrich, 1984), and no vertical displacement postdating deposition of an early to middle Pleistocene terrace (e.g., Dethier and Reneau, 1995). Locally, there is equivocal evidence for recent subsidence (Reilinger and York, 1979) and deformation of late Pleistocene terraces (Koning et al., 2004). Koning et al. (2005) established that the PFS and Embudo fault system are not hard linked at the surface. Rather, they are connected via distributed deformation on north-to-northeast-striking normal faults that displace late Quaternary pediment gravels. No paleoseismic data exist for the Embudo fault system.

METHODS

This study is based on field mapping of offset geologic markers, laboratory measurement of scarp heights from a digital elevation model (DEM) (Carey and Cole, 2002), and borehole drilling. We mapped bedrock and surficial geologic units in the field at a scale of 1:1200, using topographic base maps with 0.6 m contours derived from a DEM with a 1.2 m grid, based on a LIDAR (light detection and ranging) survey performed in 2000 (Carey and Cole, 2002). Comparison of the LIDAR survey with global positioning system (GPS) and total station surveys (Gardner et al., 1999) reveals that >90% of the LIDAR data have better than 0.6 m horizontal positional accuracy and better than 0.3 m vertical positional accuracy relative to independent

data (Carey and Cole, 2002), and meet national map standards. The geologic map shown in Animation 1 was created from digitized versions of the field geologic maps described above using ArcMap computer software (copyright ESRI).

Profiles of along-strike variation in throw were derived using several approaches. First, throw was measured in the field on the basis of displaced contacts of Bandelier Tuff subunits. Second, in areas beyond the limits of detailed mapping, throw was measured on the displaced top of the Bandelier Tuff using scarp height as a proxy. Scarp height in the Bandelier Tuff has been shown to be a reasonable approximation of stratigraphic separation on these rocks in this area (Gardner et al., 2001). Using a LIDAR 1.2 m grid (Carey and Cole, 2002) in ArcMap, we differenced elevations of points on the surface of the Bandelier Tuff in the footwall and hanging wall of any given fault. Third, in areas of substantial distributed deformation, we estimated net throw by integrating the effects of tilt of bedding, folding, and small-offset faults. Where throw was measured from mapped contacts, we estimate uncertainties to be $\sim \pm 3$ m. Where throw was estimated from cross sections or by summing distributed deformation, uncertainties are more likely to be ± 5 m. Finally, estimates of throw from LIDAR data on the surface of the tuff are minima because of potential erosion on the footwall or deposition on the hanging wall.

Borehole SHB-WETF-2C (hereafter denoted borehole 2C) was drilled in April 2000 ~450 m from the base of the main escarpment of the PF as part of a seismic hazards evaluation (Fig. 3 and Animation 1) (Gardner et al., 2001). The borehole, and seven other boreholes drilled nearby during the 2000 study (identified herein with numbers), were continuously cored (a total length of ~122 m) using either a diamond coring system with air as the circulating fluid or a hollow-stem auger with a split-spoon barrel. In some zones of particularly soft material, small-diameter punch cores were taken. Detailed lithologic logs were prepared for each hole at the drill sites upon retrieval of the core and supplemented with later detailed examination of key intervals. The details of the stratigraphy and physical and geochemical basis for correlations among boreholes are presented elsewhere (Gardner et al., 2001). We describe below the stratigraphy of borehole 2C, which shows evidence for faulting.

Calibrated radiocarbon dates were obtained from eight samples of charcoal encountered in borehole 2C (Table 1). Three of these analyses were reported in Gardner et al. (2001). Samples containing discrete charcoal fragments in silty or sandy matrix were extracted from the core

and cleaned and concentrated under a binocular microscope. Five were analyzed by the accelerator mass spectrometry (AMS) method and two by standard beta counting. One bulk sample of silt contained minimal charcoal and was therefore combusted in its entirety and analyzed by AMS. Results were calibrated using the program CALIB 5.3, per the technique described in Reimer et al. (2004).

STRATIGRAPHY

The most widespread unit in the area of detailed mapping is the Pleistocene Bandelier Tuff (named and subdivided into members by Griggs, 1964), which forms the local near-surface bedrock. The Bandelier Tuff consists of two members that were erupted as a series of ash flows during enormous caldera-forming volcanic events ca. 1.61 Ma ago (Otowi Member; date from Izett and Obradovich, 1994) and 1.25 Ma ago (Tshirege Member; date from Phillips, 2004). Figure 2 shows the generalized stratigraphy of the Bandelier Tuff and associated deposits. Detailed stratigraphic descriptions are embedded in the legend of the geologic map (Animation 1).

The Tshirege Member (Qbt, Animation 1) consists of a sequence of ash-rich ignimbrites with subsidiary phenocrysts, pumice, and lithic fragments. The cooling unit stratigraphy for the Tshirege Member that we use is based largely on that established by Broxton and Reneau (1995) and later modified (Gardner et al., 1999, 2001; Lewis et al., 2002; Lavine et al., 2003). Tshirege Member cooling units are composed of numerous flow units (in some cases associ-

ated with progressive eruption of a single pyroclastic flow; e.g., Smith, 1960) distinguished by pumice zonation, pumice swarms, lithic concentrations, or thin ash or surge layers (Self et al., 1986). Cooling unit contacts in the Tshirege Member may or may not coincide with contacts between flow units (e.g., Gardner et al., 2001), but they are readily distinguished and mapped in the field due to lithologic characteristics and differential erosion as a result of variable welding (Fig. 2 and Animation 1; see embedded photos in Animation 1). In addition, previous studies have generated a substantial geochemical and mineralogical database that allows supplemental criteria for unit correlations (e.g., Gardner et al., 2001; Lavine et al., 2003).

Units within the Tshirege Member are mapped based on primary and secondary features, including, but not limited to, welding, devitrification, vapor-phase alteration, and oxidation and relative content of phenocrysts, pumice, and lithics. Postdepositional physical changes (e.g., oxidation, devitrification, and vapor-phase alteration) are especially useful in distinguishing subunits of Qbt1. Because phenocrysts vary predictably in quantity and grain size among units Qbt3, Qbt3t, and Qbt4 (defined in Fig. 2 and Animation 1), phenocryst content is an important criterion for distinguishing among these units. Also, Qbt3 is exceptionally lithic rich, as its eruption coincided with caldera collapse, vent flaring, and ejection of considerable breccia (Kite, 1985). Across most of the Pajarito Plateau, sequences of two or more Tshirege Member subunits are present in thicknesses that produce topographic breaks in slope that can be identified readily in the LIDAR data.

RESULTS

Central Pajarito Fault Stratigraphy and Fault Zone Structure

Two subunits of the Tshirege Member (Qbt3t and Qbt4) were encountered in the seismic boreholes (Gardner et al., 2001). Subunit Qbt4 is ~14 m thick in borehole 1. The thickness of Qbt3t in the boreholes was not determined, as the base of the unit was not penetrated. In most of the boreholes, a sequence of nonwelded ash and surge beds between physically recognizable Qbt3t and Qbt4 has been geochemically correlated with Qbt4. Thickness varies from 0.3 to 1.2 m.

The top of borehole 2C consists of 4.2 m of fill and underlying soil and 9.4 m of tuff unit Qbt4. At a depth of 13.7 m, the tuff is underlain by finely laminated sands, silts, and clays with abundant charcoal (Fig. 4). The contact between the tuff and laminated sediments is horizontal, and no disruption of layering in the sediments is evident. Radiocarbon dates obtained from this sedimentary interval are stratigraphically consistent (Table 1 and Fig. 4).

Sediments from the top of the section to depths of ~17.4 m, dated as ca. 1.3–9.0 cal ka old, are not deformed. Between depths of ~17.4 m and 23.6 m (total depth of the borehole), sediments dated as ca. 11.0 cal ka old and older are deformed by centimeter- to millimeter-scale, high-angle normal faults. Clay-rich sediments at ~19.8 m depth exhibit strong foliation that dips at ~60° (Fig. 4). These foliated clays, examined by petrographic and scanning electron microscopy, show evidence for cataclasis,

TABLE 1. ¹⁴C RESULTS FROM BOREHOLE SHB-WETF-2C

Beta sample number	Depth in borehole (m)	Beta Analytic results				Calib 5.3 results	
		¹⁴ C yr BP	Intercepts cal yr B.P.	cal yr B.P. (2σ)	δ ¹³ C‰	cal yr B.P. (2σ; rounded to nearest 10)	Preferred age, cal yr BP (rounded to nearest 100)
175385	13.9	1330 ± 40	1270	1300–1180	-23.1	1310–1180	1300
143830	14.2	6330 ± 50	7260	7330–7180	-22.0	7420–7380, 7380–7350, 7330–7160	7300
143831	14.9	7450 ± 50	8365	8410–8205	-22.8	8370–8180	8300
175386	15.2	7420 ± 50	8200	8350–8160	-22.3	8370–8160, 8080–8070	8300
175387	16.0	7670 ± 40	8420	8530–8390	-24.9	8540–8400	8400
143832	17.2	8070 ± 50	9010	9095–8970, 8915– 8865, 8830–8970	-22.5	9130–8770	9000
175388	17.7	9550 ± 40	11,050, 10,970, 10,760	11,100–10,700	-23.3	11,090–10,920, 10,900–10,710	11,000
175389	17.8	12,160 ± 40	14,120	15,240–14,700, 14,340–14,070, 13,920–13,850	-22.2	14,140–13,880	14,000

Note: Results from samples 143830 and 143831 are from Gardner et al. (2001). All samples analyzed by accelerator mass spectrometry radiocarbon dating at Beta Analytic. Results calibrated using the program CALIB 5.3, according to techniques described in Reimer et al. (2004). cal—calendar; B.P.—before present.

including weak dimensional preferred orientations of sand-sized grains, well-developed preferred orientations of clay minerals, as well as parallel grooves in clay. Cataclastic lineations in this interval are presumably parallel to the slip direction, although the exact attitude of the fault is not known. Laminated sediments above and below the foliated clays exhibit distributed deformation from a depth of 17.4 m to bottom of borehole.

Sedimentation rates vary markedly in the core (Fig. 4). For the time period 9.0–7.3 ka ago, the average sedimentation rate is ~2 m/ka (with values ranging from 0.7 to 8.0 m/ka). From 14.0 to 11.0 ka and 7.3–1.3 ka ago, the

rates are nearly two orders of magnitude lower. We observed grain-size changes from silty clay (bottom of borehole up to 18.6 m depth) to pebbly silt (~18.6–16.2 m), to fine to coarse sand (~16.2–13.7 m). The change from silty clay to pebbly silt coincides with an upward change in the lithology of isolated angular breccia clasts (as long as 6 cm) of welded tuff from dominantly Qbt3t to dominantly Qbt4. However, neither grain size nor this change in lithology of clasts appears to correlate with changes in sedimentation rate.

We interpret the laminated sediments in the lower part of borehole 2C (Fig. 4) as having been deposited in flowing and ponded water in

an open fissure created by dip slip and opening (dilation) on a high-angle normal fault. A fissure-opening rupture occurred sometime prior to ca. 14.0 ka ago. A faulting event between ca. 11.0 ka and ca. 9.0 ka ago deformed the fissure fill sediments and further dilated the fault. Erosion of host rock at the margins of the fault, in particular the ash and surge sequence at the base of unit Qbt4, likely created more opening of the fissure. Deposition of fissure fill continued until ca. 7.3 ka ago, at which point the fissure had completely filled. The hiatus in deposition between ca. 7.3 ka and ca. 1.3 ka ago and then continued sedimentation up to the base of the tuff suggest further dilation at or before ca. 1.3 ka ago. Relative elevations of stratigraphic contacts in the boreholes imply that the fault that intersects borehole 2C is an east-dipping normal fault with at least 2 m of down-to-the-east stratigraphic separation (Gardner et al., 2001).

LOCAL GEOMETRY OF THE PAJARITO FAULT SYSTEM AND VARIATION IN THROW VERSUS LENGTH

In this section, we lay the groundwork for interpreting the mechanics of the PFS by describing geometric aspects of the principal structures. Although the focus of detailed mapping was the north-central part of the PFS, we first discuss the major features of the southern PFS. We have constructed a throw-length profile (Fig. 5) that is based on Banelier Tuff as the time-stratigraphic marker for measuring separation. Therefore, our measurements are limited to outcrops of the tuff, which extend as far south as Tent Rocks, ~6 km northwest of Cochiti Pueblo, along the west splay of the PF (Fig. 3). Some previous workers have similarly placed the southern end of the PFS near Cochiti Pueblo (Fig. 3; e.g., Wong et al., 1995; Smith and Kuhle, 1998; Smith et al., 2001) based on its surficial expression. Outcrops of Banelier Tuff provide continuous throw data as far as the north end of the northern Pajarito fault, 3 km north of Santa Clara Canyon.

Southern Pajarito Fault (Cochiti Pueblo to St. Peter's Dome): Two Principal Splays

From Cochiti Pueblo to St. Peter's Dome (Fig. 3), the PFS consists of numerous short faults, all of them considered part of the PFS but in some cases given other names for ease of reference (e.g., Dixon, Cochiti, and Sanchez faults). Throw for the two principal splays of the PF south of Water Canyon, the west and east splays, varies in a nonlinear fashion along strike

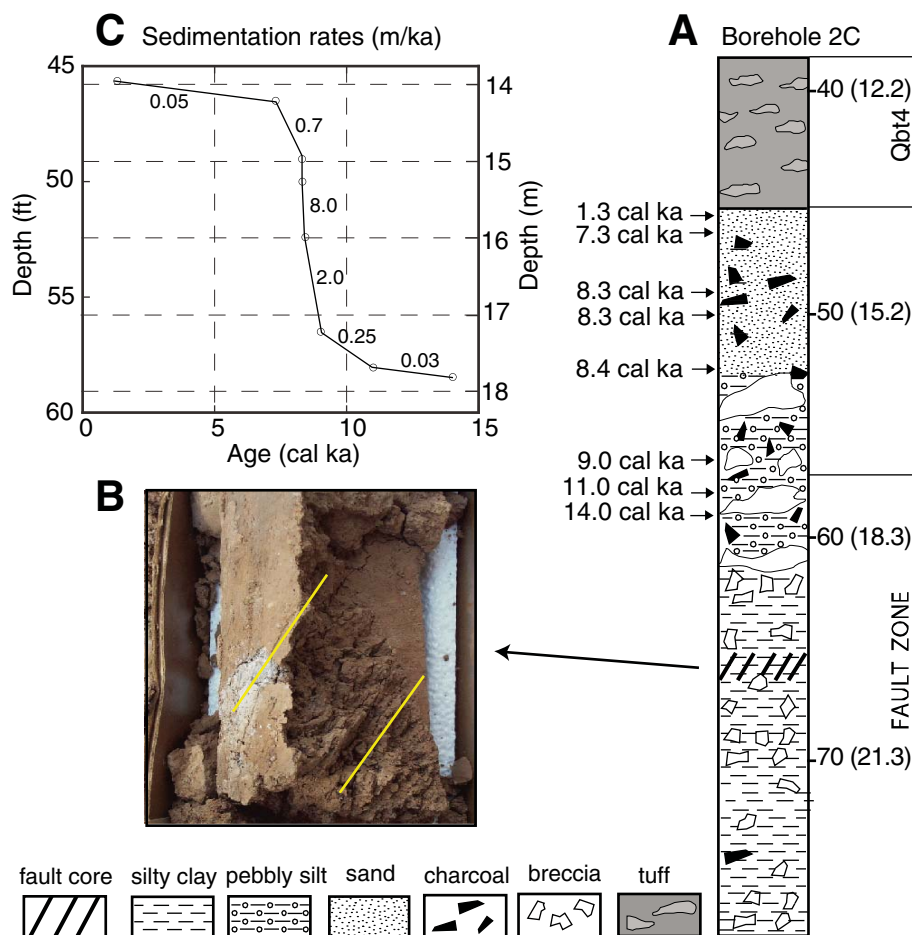


Figure 4. (A) Stratigraphy of lower part of borehole 2C (location shown in Fig. 3 and Animation 1). Banelier Tuff contacts are based on a combination of petrographic and geochemical data (Gardner et al., 2001). (B) Photograph shows steeply dipping, foliated silty clays from ~20.0 m depth in borehole 2C. Yellow lines show dip of foliation. Intensity of cataclasis suggests that the interval from 19.8 to 20.1 m is the core of a fault. Borehole core diameter is ~9 cm. (C) Depth versus calibrated age for ^{14}C samples from borehole indicates sharp increase in sedimentation rate between 11.0 cal ka ago and 9.0 cal ka ago and sharp decrease between 7.3 cal ka ago and 1.3 cal ka ago. Inflections in curve coincide with faulting events identified in core at depths of ~17.4 m and ~14.6 m.

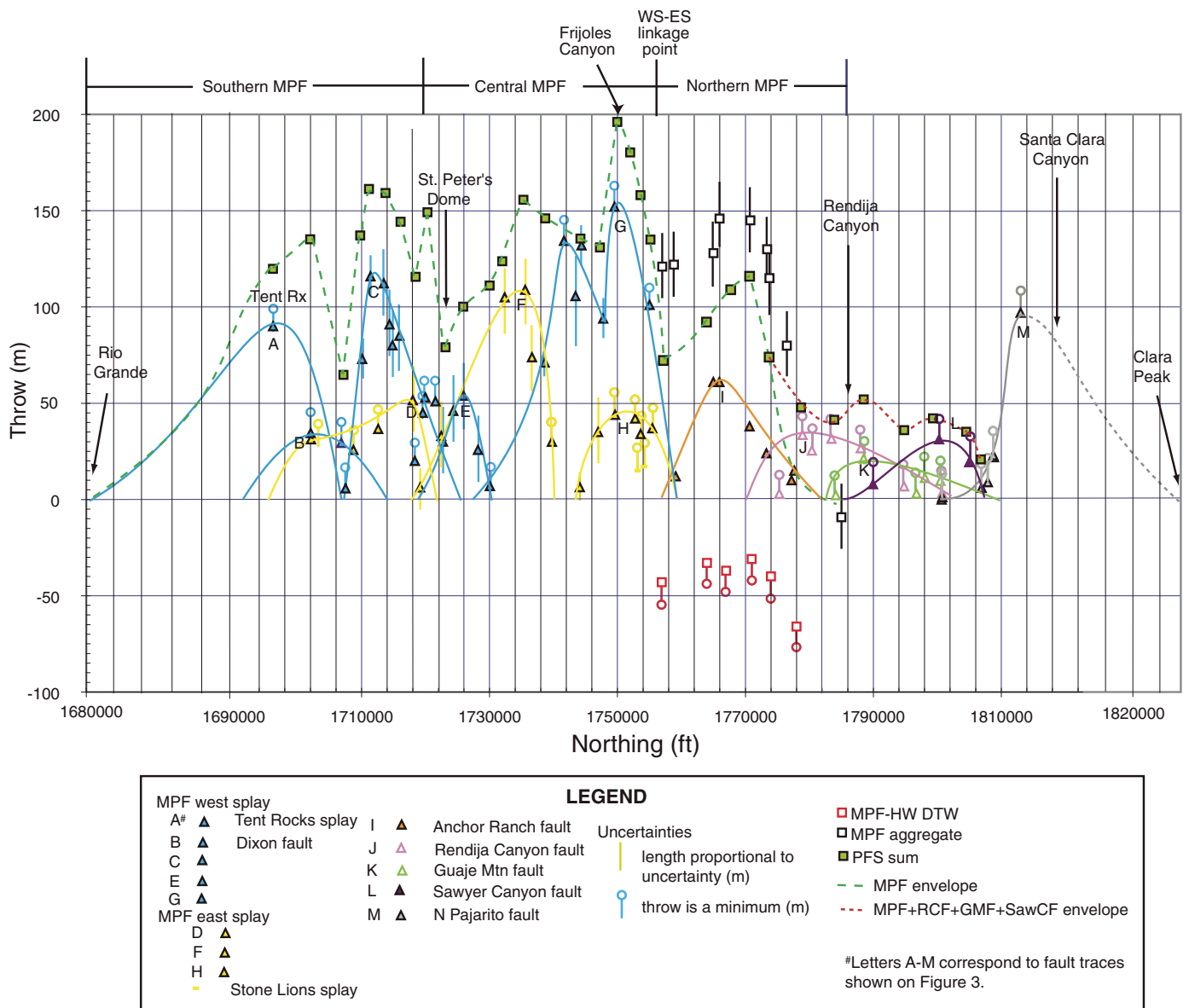


Figure 5. South-to-north profile of the Pajarito fault system (PFS) showing variation in throw with distance along the fault system. Measurements of throw on individual faults are plotted as triangles, summed distributed deformation is plotted as squares, and total throw is plotted as dashed lines. Based on map patterns of faults (few if any faults form a V across canyons in map view), we assume that throw is approximately equivalent to dip separation. All faults are plotted with positive throw, although some are antithetic and offset geologic units down to the west (dtw). Observed dtw distributed deformation in the hanging wall of the PF is plotted as negative throw only to make these measurements easier to see. Measurements by other investigators are incorporated where land access issues prevented visiting sites or where no new data on contacts were available. The best measurement available for throw on the Santa Clara Canyon fault is by Golombek (1981), who estimated ~100 m down-to-the-east (dte) on Bandelier Tuff; we have not been able to confirm that estimate due to access restrictions. We estimate 107 m distributed dte throw at Quemazon Mesa (Animation 1), 115 m south of Los Alamos Canyon, 145 m between Pajarito Canyon and Cañon de Valle, and 120 m at Water Canyon. Summed throw in this sector includes estimates made by Carter and Gardner (1996) on the Rendija Canyon fault (RCF) and Guaje Mountain fault (GMF) and by Gardner et al. (1999) on the southern tail of the RCF. The estimate of 90 m dte throw on the west splay near Tent Rocks comes from Smith et al. (2001). Distance grid is in State Plane coordinate system, New Mexico Central Zone, NAD83. Included here are several strands not discussed in text, i.e., the Stone Lions splay (Reneau, 2000) and the Dixon fault (Aby, 1997). MPF aggregate is the sum of dtw and dte throw on small-displacement faults in the footwall block of the MPF; it does not include throw on the MPF, where that is delimited by cross sections. PFS sum includes throw on all mapped splays of the fault system where a reliable estimate of throw is available. HW—hanging wall.

(Fig. 5), resulting in sawtoothed profiles, indicating that this section of the PFS is composed of short segments ~8–12 km long, each of which has maximum throw near the center that tapers off more or less symmetrically at both ends. Where throw is low for the PF west splay, it is high for the PF east splay, except at St. Peter's Dome and Frijoles Canyon, as seen in Figure 5.

The west splay of the PF is sinuous, having a 10-km-long north-striking southern section, an 8-km-long northeast-striking central section, and a 10-km-long north-striking northern section (Fig. 3). Throw varies along strike, reaching lows at several points along the northeast-striking section and adjacent to St. Peter's Dome (Fig. 3, location E), where the fault bends sharply to the north. Where the west splay crosses Cochiti Canyon (Fig. 3, location C), it offsets a fluvial terrace (estimated to be ~85 ka old) ~6 m down to the east (Aby, 1997). The correlative Quaternary terrace in Peralta Canyon, just south of Tent Rocks, is displaced 14 m down to the east (Smith et al., 2001).

The east splay is generally north-striking except at its northern end, where it curves westward and connects with the west splay north of Frijoles Canyon (Fig. 3). The southern end of the east splay is the 8-km-long Sanchez fault (Fig. 3; Minor et al., 2006). Based on strong aeromagnetic expression (Minor et al., 2006), the Sanchez fault has been traced another ~10 km south of the Rio Grande. No Bandelier Tuff is exposed there to indicate if that part of the fault has been active since 1.25 Ma ago. The Sanchez fault has its maximum throw of 51 m where it steps to the west to another strand of the PF east splay. In the stepover are numerous topographic lineaments, identified in the LIDAR data, that compose two more or less orthogonal sets, one set parallel to the Sanchez fault and the other orthogonal to it. This area also shows a complicated pattern of intersecting stream channels. One set flows south parallel to the east splay and another set flows east, nearly orthogonal to the west splay. Complex interaction between these drainage sets reflects competition between dip domains associated with displacements on the west and east splays. Data from Aby (1997) on displaced post-Bandelier Tuff alluvial deposits along the east splay indicate surface rupture in late Pleistocene time. Near the exposed southern end of the Sanchez fault at the Rio Grande, the fault offsets a fluvial terrace (estimated to be ~250–340 ka old) ~30 m down to the east (Aby, 1997).

Central Pajarito Fault: Two Splays and a Breached Relay Ramp

This part of the PFS includes northward continuations of the two prominent west and east

splays (Fig. 3). The spacing between the two splays is ~0.9–1.5 km, except where the east splay bends westward and links with the west splay north of Frijoles Canyon. Other short, small-displacement faults have been mapped in this area, including the Stone Lions splay of Reneau (2000). At St. Peter's Dome, where the west and east splays first come into close proximity to each other (Fig. 3), there is a prominent low in throw on both splays, resulting in a pronounced deficit in cumulative throw for the fault system (Fig. 5).

The crustal sliver between the two splays is also faulted by high-angle normal faults orthogonal to the north-striking splays, resulting in a series of small horsts and grabens. Near its northern end, the east splay is associated with numerous short, small-throw normal faults that parallel the splay or strike at a high angle to it. The west splay terminates near Water Canyon in a faulted monocline (Animation 1).

Throw on the east splay varies along strike, generally in inverse relation to the west splay (Fig. 6); where throw is high on the west splay, throw is low on the east splay and vice versa. This is typical of an echelon normal fault segments (e.g., Peacock and Sanderson, 1994). Near St. Peter's Dome (center of Fig. 6), throw on the west splay is negligible; strata in the hanging-wall block of the west splay dip toward the east splay, which has its maximum throw (109 m) at this location. The horst located between the two splays is bounded to the north and south by cross faults. These horst and graben blocks have variable dips, but generally graben blocks tilt toward the west splay escarpment, whereas horst blocks tilt toward the east splay.

At Alamo Canyon, throw on the west splay is negligible, but increases rapidly to the north. At Frijoles Canyon, the west splay is north striking, and the PF is characterized by simple normal faulting, resulting in well-expressed escarpments. Maximum cumulative throw across the entire PFS occurs at Frijoles Canyon, where the west splay displaces the Qbt3t-Qbt4 contact ~155 m down to the east. The east splay displaces the same contact 40 m down to the east, for a total of 195 m (Figs. 5 and 6). The eastern splay also forms the western edge of a small ~500-m-wide graben; the fault on the east side of the graben has 30 m down-to-the-west throw on the Qbt2-Qbt3 contact.

The network of faults composing the central PFS appears to be a left-stepping, synthetic relay structure (e.g., Trudgill and Cartwright, 1994). The overall geometry suggests that the zone between the two splays is a relay ramp (e.g., Crider, 2001). The main fault here is the west splay, which is considered active (e.g., Boden, 1980; Gardner and House, 1987; Aby, 1997).

The distributed faulting near the north end of the east splay (Fig. 3, near location H) may represent deformation ahead of a propagating fault tip that occurred before the east and west splays linked. As such, these small faults are probably inactive. The linkage point between the splays coincides with a dramatic displacement gradient (Fig. 5). Throw decreases from the ~200 m maximum at Frijoles Canyon to ~75 m at Water Canyon. The geometry of linkage between the two splays is consistent with results of Crider (2001), in which left-stepping echelon faults with left-oblique slip tend to breach the hanging wall of the rear segment (the west splay) as stresses are high ahead of the tip of the propagating front segment (east splay). Left-oblique slip produces stress perturbations around the tips of left-stepping echelon fault segments that make the relay ramps releasing steps, thus favoring abandonment of the tip of the rear segment. The east-west-striking, dip-slip-connecting faults between these two splays are consistent with left-oblique slip across a releasing step and suggest that the PFS in this area is undergoing left-oblique slip.

Northern Pajarito Fault: Monoclinial Folding and Distributed Faulting in the Tip Zone

The PF north of Water Canyon is characterized by distributed normal faulting and monoclinial folding (Animation 1 and Figs. 5 and 7). The fault system in this area is right-stepping and curvilinear. It comprises numerous short north-striking splays with small displacements, monoclines, faulted monoclines, transverse faults, and a graben system at the base of the main fault escarpment (Animation 1 and Fig. 7). Maximum throw of 55 m down to the east occurs on the Anchor Ranch fault (the largely buried main fault in this sector), but associated deformation extends into the footwall block 2000 m to the west of the Anchor Ranch fault and into the hanging-wall block 2000 m to the east. Deformation of the hanging wall is well expressed topographically from just south of Frijoles Canyon to the intersection of the RCF and the PF. The hanging wall is locally deformed by antithetic faulting, monoclinial folding, and westward tilting of hanging-wall strata (Animation 1). There are notable changes in geometry from south to north in this part of the fault system. The width of the footwall deforming zone increases from south to north. Monoclinial dips are greater in the south but accommodate more displacement in the north, indicating a northward increase in the wavelength of the monocline. Monoclinial limb dips are higher at Water Canyon

(40°–66°) than at Los Alamos Canyon (34°–54°). The monoclines at Water and Los Alamos Canyons are shorter wavelength (82 m and 125 m, respectively) than the monocline at Quemazon Mesa (280 m) (Fig. 7a, sections E-E', C-C', B-B'). The graben system is ~15 km long, extending from about Frijoles Canyon in the south to Rendija Canyon in the north. The northern end is not well expressed structurally. Graben width and depth change from narrower and deeper near Frijoles Canyon to wider and shallower in the north. The geometry of the footwall deforming zone and the presence of monoclines, extensive hanging-wall deformation, northward decrease in throw and widening of the fault zone, and branching and diverging of fault strands indicate that this part of the PF is its northern tip zone (Animation 1 and Fig. 7).

COMPOSITE THROW-LENGTH PROFILE

A composite throw-length profile is shown in Figure 5, which has a total length of ~50 km (Fig. 3). The profile shows cumulative throw going to zero at both ends with a maximum (~200 m) located near the center at about Frijoles Canyon. North of Frijoles Canyon, displacement drops off dramatically, producing a pronounced displacement gradient, and reaches a minimum between Rendija and Santa Clara Canyons, before throw picks up significantly on the northern PF (Fig. 5). Between the main and northern Pajarito faults, displacement is accommodated by down-to-the-west throw on the RCF and GMF as well as down-to-the-east throw on the Sawyer Canyon fault and, possibly, on the Puye fault system east of the study

area (e.g., Koning *et al.*, 2005). As there are no outcrops of offset Bandelier Tuff along the Puye fault (Dethier, 2003), we have excluded it from our profile. The total throw (where all summed throws, whether synthetic or anti-synthetic, are positive) across the zone where the RCF, GMF, Sawyer Canyon fault, and northern PF come together is ~52 m. This appears as a prominent displacement low on the composite profile between Rendija and Santa Clara Canyons (Fig. 5).

A striking feature of the throw-length plot (Fig. 5) is that the curve for total vertical displacement shows a pronounced low on the profile at the northern end of the RCF and GMF and subsidiary lows at St. Peter's Dome and directly north of Tent Rocks. Adding distributed deformation west and southwest of the city of Los Alamos (including PF hanging-wall

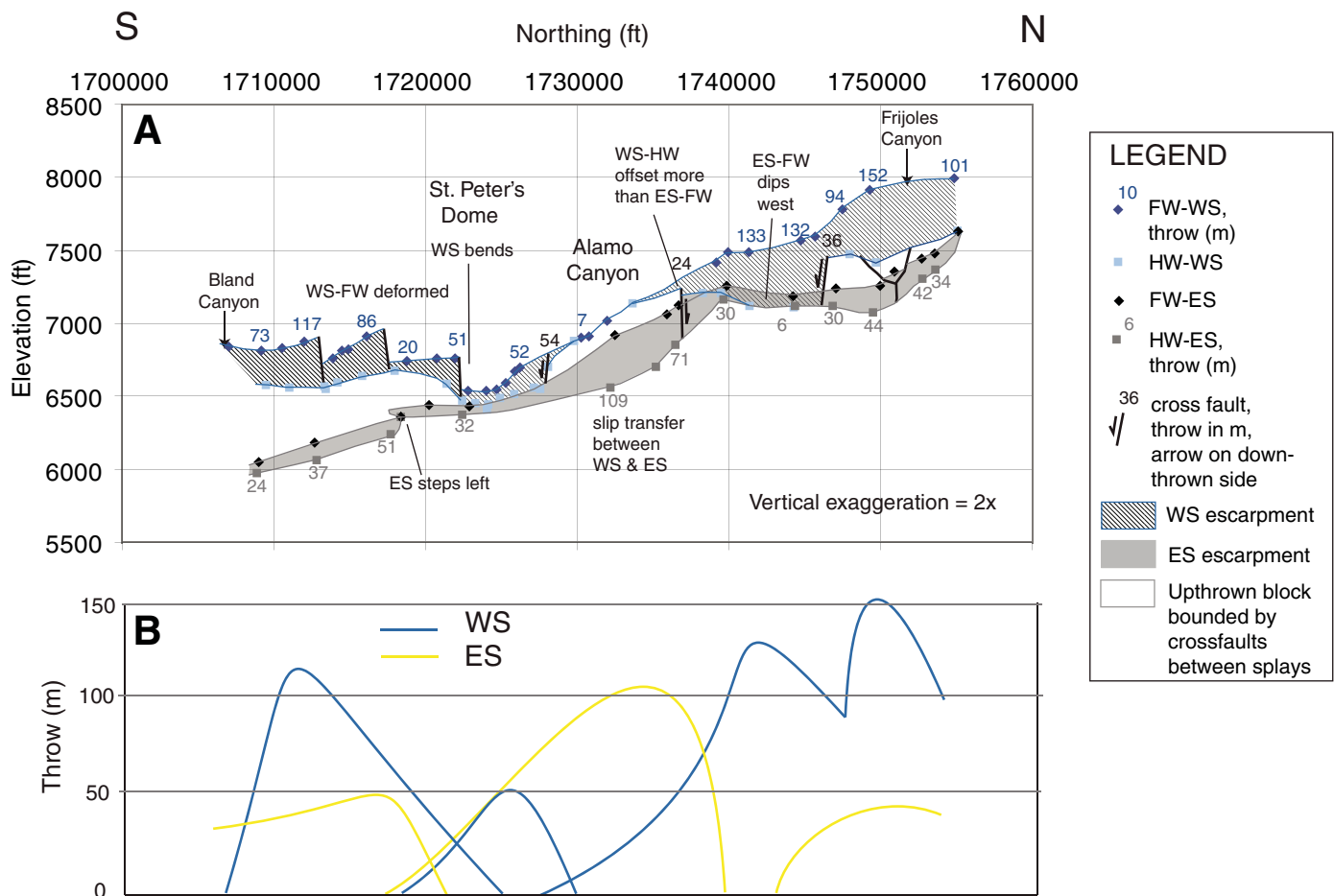


Figure 6. Plots of fault escarpment elevation and corresponding throw versus location along fault traces, showing strain partitioning along the central part of the Pajarito fault (PF). Plots are drawn looking west at the west splay (WS) and east splay (ES) escarpments. (A) Squares and diamonds show elevation of the top of tuff on the hanging wall (HW) and footwall (FW), respectively, of both splays. White areas between the splays are relatively upthrown blocks bounded by cross faults within the zone between the two splays. (B) Partitioning of throw is most obvious near center of figure where west splay has no throw and east splay, by contrast, has more than 100 m down-to-the-east throw.

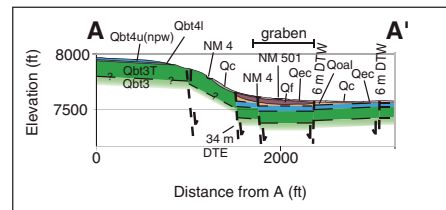
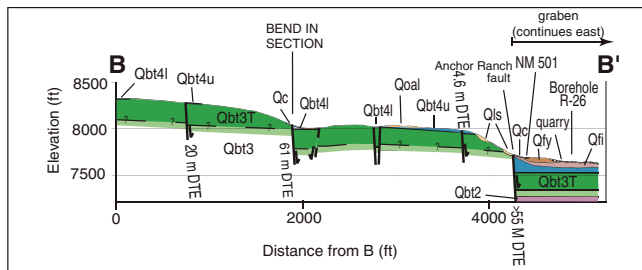
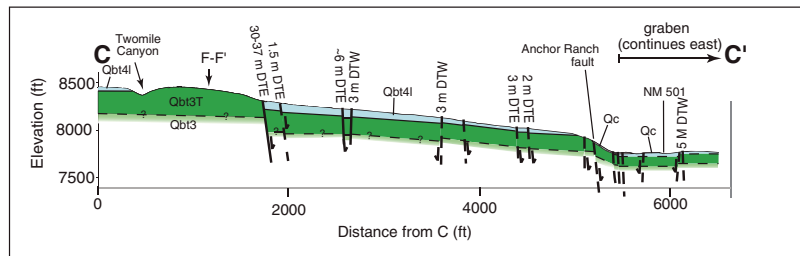
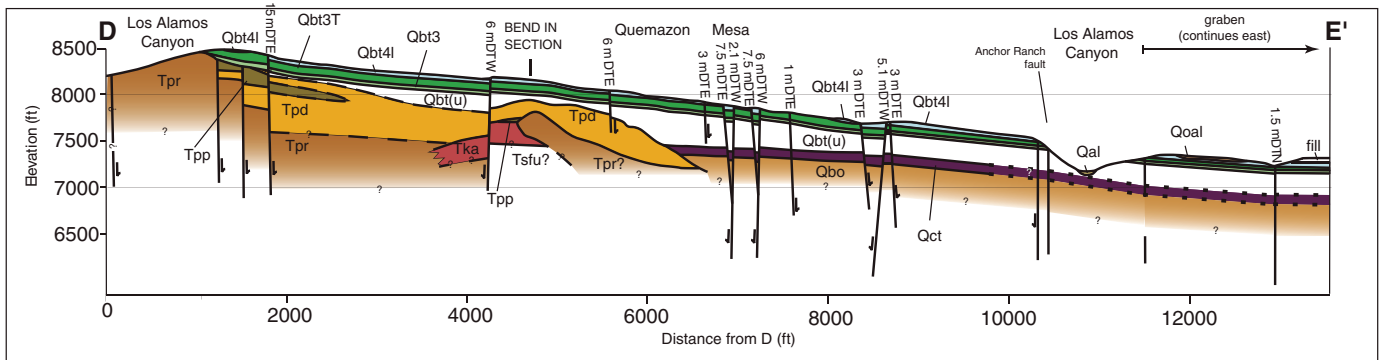
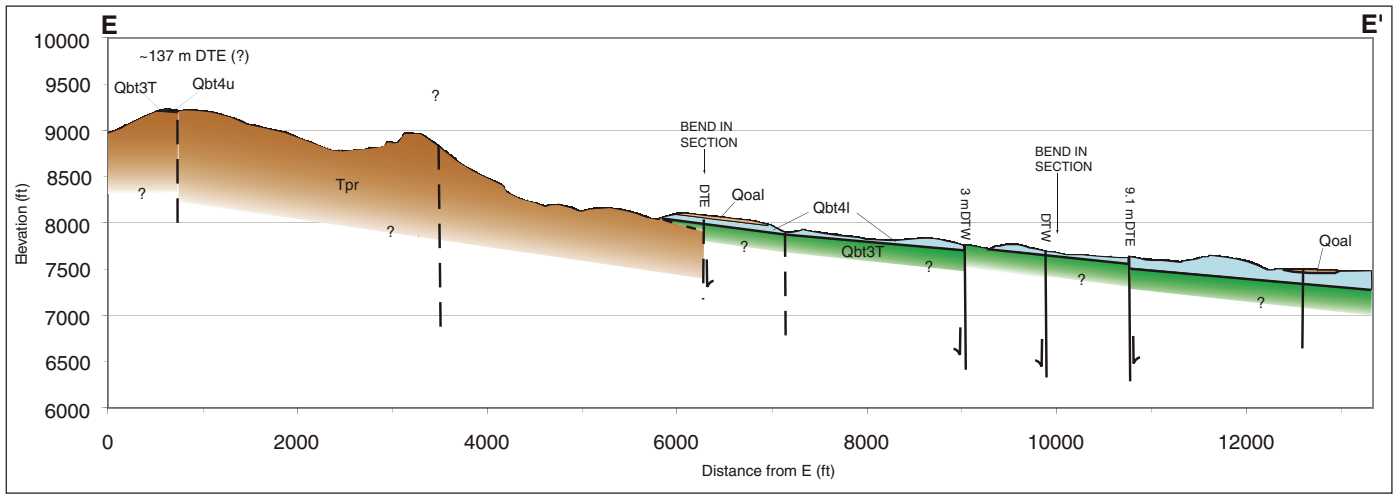


Figure 7 (continued on next page). Cross sections of the Pajarito fault system. (A) West-east cross sections spanning the Pajarito fault system. DTE—down to the east.

A

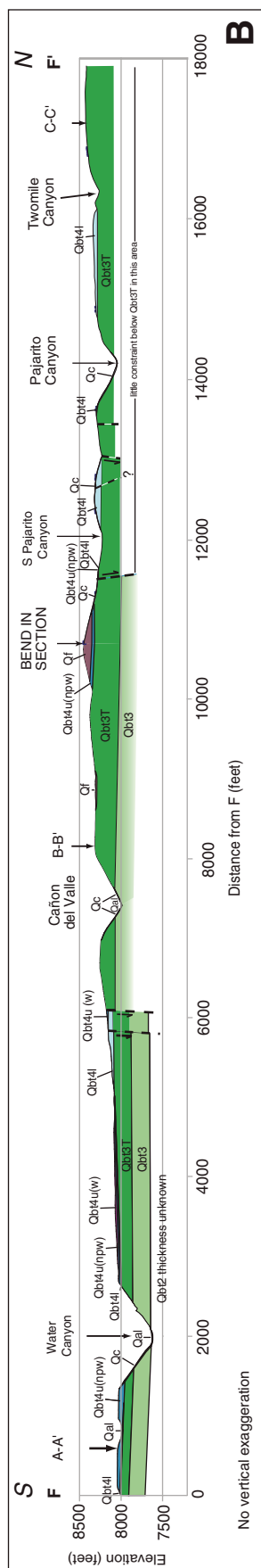


Figure 7 (continued). (B) South-to-north cross section. Locations of sections are indicated in Figure 4. See text for discussion. No vertical exaggeration. Based on map patterns of faults (few if any faults form a V across canyons in map view), we assume that throw is approximately equivalent to dip separation.

deformation; Fig. 5) does not eliminate the more northern displacement low. At St. Peter's Dome, throw on mapped faults totals only ~80 m. Near Tent Rocks, throw totals only ~70 m. However, there are small faults located west of the west splay that do not cut Bandelier Tuff (Gardner and House, 1987), but may fold it slightly down to the east. There are also suggestions in the LIDAR data of more faults to the west and east of the PF. The footwall and hanging-wall blocks along this sector may be more deformed than recognized previously. We further discuss these structurally complex zones in the following.

Nearly all faults in the PFS have asymmetric throw-length profiles. On the Rendija Canyon and Guaje Mountain faults, the throw maxima are located near the south end, resulting in large throw gradients toward the PF. The Sawyer Canyon fault, however, has its throw maximum closer to its north end, resulting in a large throw gradient toward the northern PF. The northern PF, in turn, appears to have its displacement maximum shifted toward the PF, but we have few data to determine the shape of its profile.

DISCUSSION

Paleoseismic Event Chronology

We interpret the stratigraphic and structural evidence in borehole 2C as resulting from subsidiary faulting associated with surface ruptures in the Pajarito fault system. At least three events seem to be required by stratigraphic, structural, and geochronological relations as follows: event 1, older than 14.1 cal ka; event 2, older than 9.0 cal ka and younger than 11.0 cal ka; and event 3, older than 1.3 cal ka and younger than 7.3 cal ka. Event 3 is similar in timing to the youngest event in the PFS (McCalpin, 2005), the preferred age for which is ca. 1.4 cal ka. Event 2 is similar in timing to the preferred age estimate for a surface-rupturing earthquake on the RCF (ca. 8.1 cal ka or older; Wong et al., 1995; Kelson et al., 1996). Evidence from a trench in the tip zone of the main PF for an event after ca. 10.5 cal ka ago, possibly near ca. 8.6 cal ka ago (Reneau et al., 2002), is also suggestive of surface rupture during the same event. The dramatic increase in sedimentation rate ca. 9.0 ka ago in borehole 2C is consistent with dilation, possibly due to a seismic event. Event 1, with only a minimum age constraint, is too poorly constrained to attempt a correlation with other dated seismic events in the PFS.

These data, interpreted in light of previous paleoseismic work in the PFS, add weight to the argument for three Holocene events, one ca.

1.4 cal ka ago on the PF (McCalpin, 2005), a second 6.5–5.2 ka ago on the PF (McCalpin, 2005) that is consistent with an event 6.5–4.2 ka ago on the GMF (Gardner et al., 2003), and a third ca. 9 ka ago on both the PF and the RCF (Wong et al., 1995; Kelson et al., 1996; Reneau et al., 2002; this study). The simplest explanation for the available evidence is simultaneous rupture on the PF during the most recent event on the other two faults, and establishment of structural linkage of the faults of the PFS to one another. When this occurs, the resultant seismic moment and therefore the earthquake magnitude must be larger than when the PF ruptures alone. Recognition that the Rendija Canyon and Guaje Mountain faults are structurally linked to the PF simplifies the number of rupture scenarios that must be considered in assessment of seismic hazard (Wong et al., 2007).

Fault Tip

As detailed here, the geometry of the extensional monocline associated with the central PF fault tip varies systematically from south to north. Similar to the Nopolo structure in the Gulf extensional province of Baja California (Willsey et al., 2002), the amplitude of the monoclinical segments varies, reaching a maximum (75 m) near the northern tip at Quemazon Mesa, where the Anchor Ranch fault does not break the surface and the monocline accommodates all of the down-to-the-east throw.

Where the Anchor Ranch fault breaks the surface to the south, it does so at the lower monoclinical hinge. A graben at the base of the escarpment is present along the PF from Water Canyon to Los Alamos Canyon, with the Anchor Ranch fault and/or the monocline forming the west side of the graben. This contrasts with the Nopolo structure, where steep to moderate dips persist well out into the hanging wall (Willsey et al., 2002).

Like other extensional monoclines (e.g., Withjack et al., 1990; Hardy and McClay, 1999; Withjack and Callaway, 2000; Willsey et al., 2002), those associated with the PF formed by propagation of normal fault tips. As the Anchor Ranch fault propagated upward, breaking the surface between Water and Los Alamos Canyons, growth of the fold presumably ceased. Spatial trends in the geometry of the monocline appear to be a proxy for time in that more southern sections, with higher limb dips, underwent faulting of the monocline earlier than more northern sections. Overall, these trends suggest northward propagation of the PF tip from Water Canyon to Rendija Canyon, a distance of ~8 km, since the tuff was deposited.

Fault Interaction and Linkage

The short lengths and antithetic dips of the RCF and GMF, and their location in the step-over between the PF and the northern PF, suggest that they are subsidiary to the larger displacement east-dipping faults. The paleoseismic data corroborate this. To visualize the interaction of these synthetic and antithetic faults at depth, we have constructed schematic cross sections at a number of points along the PFS (Fig. 8) as well as a three-dimensional conceptual model (Fig. 9). In Figure 8 cross sections, we depict a range of reasonable dips for several faults (i.e., 45°–75° for the PF and 60°–90° for the RCF and GMF). The map patterns of faults in the PFS show that most are high angle, nearly vertical, at the surface; few if any faults form a V across canyons in map view. Except in the case where the PF is steep and the RCF and GMF are vertical, the antithetic faults intersect the PF at a relatively shallow depth. Figure 9 shows our interpretation of the fault geometry in the subsurface. As the principal bounding faults of the Española basin, the PF and northern PF are probably crustal-scale faults (dipping at high angle down to the base of the brittle crust; Baldrige et al., 1995), whereas the RCF and GMF are subsidiary but important, in that they bridge the gap, in the subsurface at least, between the main and northern strands of the Pajarito fault.

The RCF has a strongly asymmetric throw-length profile with maximum throw and a sharp displacement gradient near its southern end (Fig. 5). The GMF is similar. The PF, by contrast, has a steep displacement gradient near its northern end. In its tip zone, displacement is distributed onto numerous short splays rather than one main fault, and monoclinical folding accommodates part of the strain. The shapes of the fault throw profiles are typical of situations in which elastic interactions occur between neighboring faults (e.g., Peacock and Sanderson, 1991; Dawers and Anders, 1995); interacting faults display profiles with maximum displacement skewed toward the overlapped end of the fault trace, and the displacement gradients toward the tips of overlapping faults are steeper than non-overlapping tips (e.g., Peacock and Sanderson, 1991). The overlap between the PF and RCF, their pronounced asymmetric throw gradients, and the distributed deformation at the northern tip of the PF and southern tip of the RCF indicate fault, and thus stress, interaction, which is corroborated by the paleoseismic data. In two of three Holocene earthquakes, the PF ruptured with one of the overlapping antithetic faults.

Fault interaction has significant implications for seismic hazards. The probability of an earthquake rupture propagating from one

fault to another increases with the degree of stress interaction between the faults (Scholz and Gupta, 2000). When the PF and the RCF rupture together, the seismic moment and therefore the magnitude should be substantially larger than when the PF ruptures alone. Paleoseismic data show that the PF sometimes ruptures alone and sometimes ruptures with either the RCF or the GMF. This pattern may be due to stress interactions. If the RCF ruptures, the stress on the GMF may decrease, because it would be in a zone of reduced stress (e.g., Caskey and Wesnousky, 1997; Crider, 2001). The converse is also likely true. However, when the PF ruptures, stress would increase along strike, likely pushing the RCF or GMF closer to failure.

Based on its probable interaction with the RCF and GMF, the PF may no longer propagate northward, although it may continue to propagate upward through the Bandelier Tuff. Rather, the PF, RCF and GMF are slowly accumulating displacement in the zone of overlap between the faults, and thus gradually filling in the local displacement deficit relative to the system as a whole (Fig. 5). This is a fault system of short segments that have just recently linked together; the near-surface displacement asymmetries have not yet evened out.

Like many other normal faults, the PFS is corrugated (e.g., Ferrill et al., 1999), having multiple overlapping sections 8–14 km in length and ending in curved or angular bends. The general absence of hanging-wall rollover, or reverse drag, except between Frijoles and Pajarito Canyons, suggests that fault corrugations generally plunge downdip parallel to a planar fault surface (Fig. 9). As available paleoseismic data demonstrate that the PF, RCF, and GMF are mechanically linked and sometimes rupture together, fault growth likely occurred through physical linkage of overlapping segments by processes of updip and lateral propagation of echelon fault tips and formation of new connecting faults (e.g., Peacock and Sanderson, 1994; Trudgill and Cartwright, 1994; Tavarnelli and Pasqui, 2000). The displacement gradients at the interacting ends of the PF, RCF, and GMF, and other asymmetries in the throw-length profile associated with bends in the fault system result from physical linkage of segments (Fig. 9).

Growth by linkage of fault segments has implications for the regional strain rate through time in this part of the Rio Grande rift. Numerous studies have shown that slip scales linearly with fault rupture length (e.g., Scholz, 1982; Wells and Coppersmith, 1994). One well-known model for fault growth holds that faults become larger due to systematic increases in rupture length and maximum displacement (e.g., Cowie and Scholz, 1992).

Faults grow by accumulation of slip over millions of years and by tip-line propagation and linkage of initially isolated faults. As length increases, displacement increases. As a fault propagates along strike, its surface area also increases, meaning that seismic moment must increase through time as well, because moment is a function of fault plane area (Nicol et al., 1997). The implication is that the regional strain rate also increases with time, since strain rate increases with increasing seismic moment. Constant regional strain rate may be achieved if fault lengths are established early and lateral propagation is slowed by fault interaction or by a temporal decrease in the number of active faults, such that strain is concentrated on fewer faults that get bigger through time (Nicol et al., 1997). If the regional deviatoric stress is constant through time, then strain may concentrate on a few larger faults, and smaller faults become inactive. This may be a reason why the early Rio Grande rift basins were generally broader than the present basins (e.g., Chapin and Seager, 1975). This may be why the rate of activity on the Cañada de Cochiti and Cañones fault zones (Fig. 1) slowed as late Miocene extension at the Española basin margin focused on the PFS (e.g., Gardner and Goff, 1984).

Fault Bends and Intersections

As noted here, the PFS has three principal bends that coincide with throw deficits (one concave, beginning south of Rendija Canyon; one convex, at St. Peter's Dome; and the third concave, north of Tent Rocks) (Figs. 3, 5, and 9). In the bend beginning near Rendija Canyon (section S5, Fig. 8), the antithetic RCF and GMF likely abut the PF in the subsurface. The depths at which they intersect depend on the dips of the faults. Unless all faults are vertical, the intersections should be at less than 10 km depth (Fig. 8).

Where faults intersect, they can lock, resulting in a geometrical complication that in many cases is a strong part of the fault system with increased resistance to earthquake rupture propagation (e.g., Aki, 1979; Susong et al., 1990). Such fault intersections may not always act as barriers, however. Elastic strain can build within them, eventually nucleating a rupture or loading the barrier close to its yield strength, setting it up for possible triggering by a near-field or far-field earthquake (e.g., Caskey and Wesnousky, 1997; Gomberg and Johnson, 2005).

Similarly, bends can also act as nucleation points. Some of the many examples in the literature of unilateral and bilateral ruptures with subevents that initiated at bends or where two normal fault segments intersect include the 1981 Gulf of Corinth (Greece) earthquake

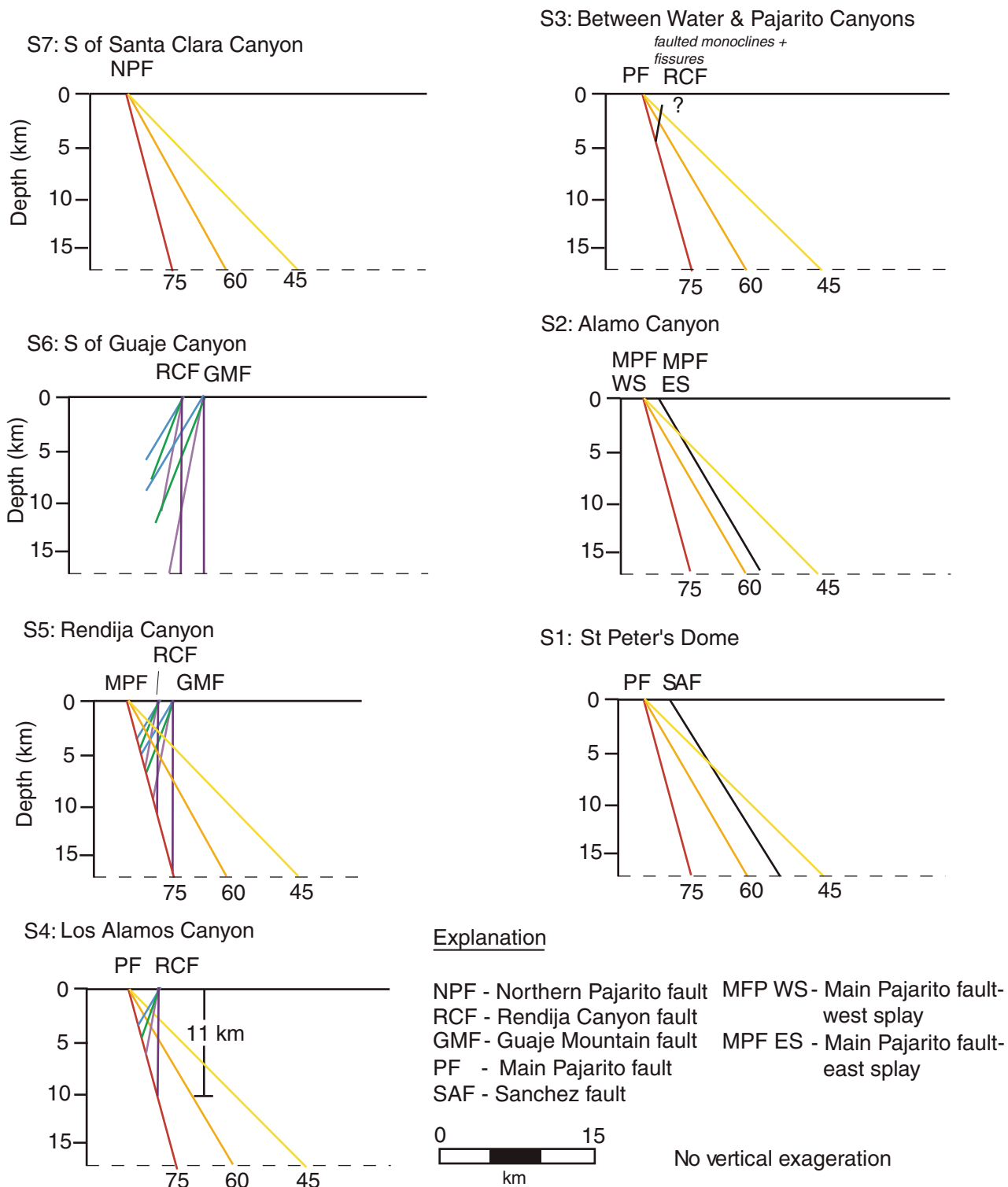


Figure 8. Diagrammatic two-dimensional cross sections showing along-strike variations in range of possible dips for the main Pajarito fault (MPF), Rendija Canyon fault (RCF), Guaje Mountain fault (GMF), and northern Pajarito fault, and their geometric relations in the subsurface. Scale bar on left side of each panel indicates depth (km) below surface. Numbers shown adjacent to faults are dips. Colors added for clarity; red-orange-yellow indicate dips of 75°, 60°, and 45°, respectively, on the MPF, and purple-violet-green-blue indicate dips of 90°, 80°, 70°, and 60°, respectively, on the RCF and GMF. Locations of sections S1 through S7 are shown in Figure 3.

(Vita-Finzi and King, 1985), the 1984 Lazio-Abruzzo (Italy) earthquake (Westaway et al., 1989), the 1959 Hebgen Lake (Montana, USA) earthquake (Doser, 1985), and the 1954 Dixie Valley–Fairview Peak (Nevada, USA) earthquake (Doser, 1986). In some of these cases, the ruptures failed to breach the surface between the fault segments. Of particular concern in terms of seismic hazard is irregular rupture propagation with nonuniform slip (i.e., a rupture with sub-events), which tends to enhance high-frequency waves (Aki, 1979). A possible analog for the convex bend near St. Peter's Dome on the PF is the Borah Peak horst in Idaho, which is at the convex intersection of two normal fault segments, one of which (the Lost River fault) ruptured in the Borah Peak earthquake (Susong et al., 1990). The intersection zone at the Borah Peak horst is thought to have influenced earthquake nucleation and arrest for millions of years (Susong et al., 1990). The concave bend and wide complex zone of extensional deformation

between the main and northern Pajarito faults and the RCF south of Rendija Canyon (Fig. 3) may be analogous to the Gulf of Corinth system. In the 1981 Gulf of Corinth earthquake series, warping of the surface between two normal faults resulted in strike-parallel extension and discontinuous surface fissures between the two main surface ruptures (e.g., Jackson, 1982; Vita-Finzi and King, 1985). As is the case with the PF and northern PF, the main Corinth fault failed to reach the surface across the bend, even though it may be a continuous structure in the subsurface. In systems like the Gulf of Corinth or the PFS, secondary faults, nucleating at the surface and propagating downward, might result from large near-surface stress perturbations between two principal faults.

CONCLUSIONS

The Pajarito fault system (PFS) includes the main Pajarito fault (including the west and east

splays) and the Rendija Canyon, Guaje Mountain, northern Pajarito, Sawyer Canyon, and Puye faults and associated monoclinial folds, small-displacement faults, and fissures. The geometry of the PFS varies in a complex fashion along strike. Extensional monoclines are a primary feature of the main PF at its northern tip, where the fault terminates in a series of secondary en echelon to northward-branching faults that comprise a wide zone of discontinuous, small-displacement, synthetic and antithetic faults and folds.

The main PF has a strongly asymmetric aggregate throw-length profile with maximum throw and a sharp throw gradient toward its northern end. The Rendija Canyon and Guaje Mountain faults have steep throw gradients near their southern ends. Along the central part of the main Pajarito fault, where total throw is largest, the PF consists of a series of fault-breached relay ramps where displacement is partitioned onto two principal, subparallel fault splays.

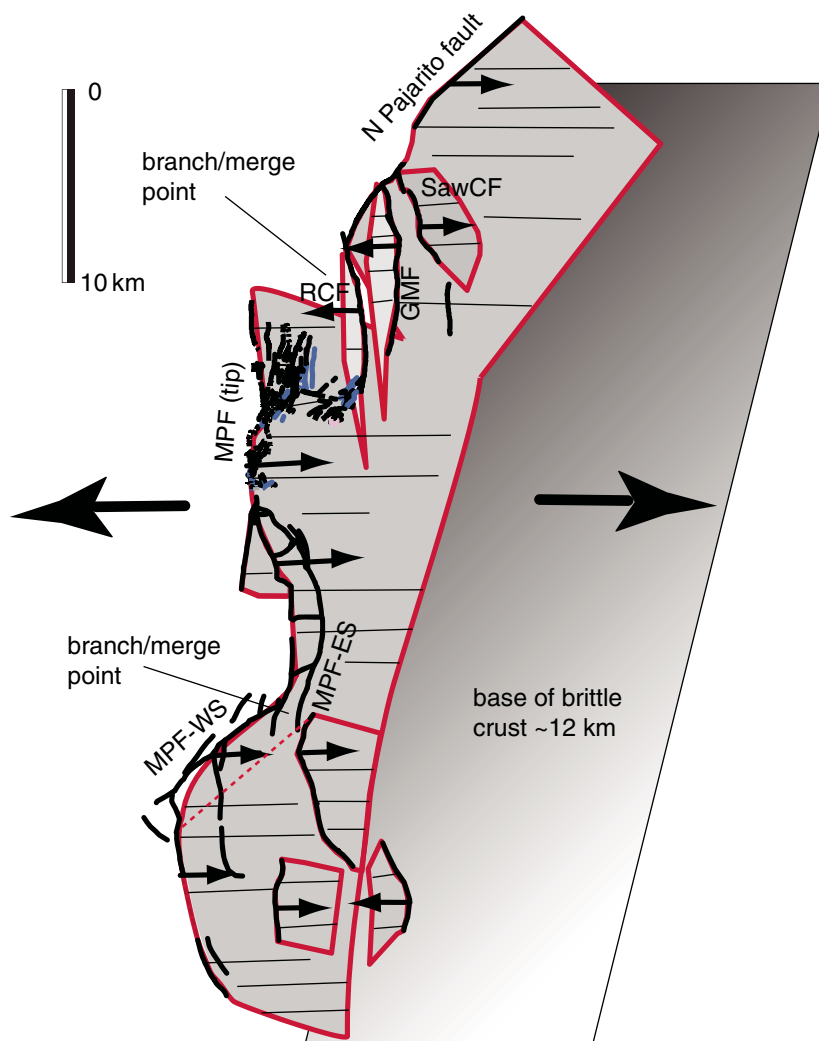


Figure 9. Three-dimensional model of the main faults of the Pajarito fault system and their geometric relations in the subsurface. The principal east-dipping fault strands are shown penetrating at a high angle to the base of the brittle crust (e.g., Baldrige et al., 1995). Large black arrows show regional extension direction (from Zoback et al., 1981). Small black arrows and thin black lines on fault planes suggest probable slip directions. Blue lines are monoclinial fold axes. Horizontal and vertical scales are the same. MPF—main Pajarito fault; RCF—Rendija Canyon fault; SCF—Sawyer Canyon fault; GMF—Guaje Mountain fault; WS—west splay; ES—east splay.

The main PF interacts structurally and mechanically with the overlapping, antithetic Rendija Canyon and Guaje Mountain faults. Interaction between the tips of the Pajarito and Rendija Canyon faults is expressed by branched secondary faults at the terminations of both faults. A marked low on the throw versus length profile of the fault system is located where these faults overlap. Between these two faults within the Diamond Drive graben, east-west–striking normal (oblique-slip?) faults have formed in the north-plunging structural ramp at the south end of the graben. The southern end of the GMF has not been mapped in detail, but its southern termination is likely to be similar to that of the Rendija Canyon fault.

The main PF appears to have propagated northward ~8 km from Water to Rendija Canyon since deposition of the Tshirege Member 1.25 Ma. It does not appear to be propagating lengthwise north of Rendija Canyon at this time, although propagation upward through the Bandelier Tuff may be continuing. Rather, the main Pajarito and Rendija Canyon faults are accumulating displacement in the zone of overlap between the faults, gradually leveling out the displacement profile of the system as a whole.

Like many other normal faults, the main PF is corrugated and its fault trace is bent, having multiple overlapping sections 8–14 km in length that strike north or northeast. Fault growth in the PFS likely occurred through linkage of overlapping segments by processes of updip and lateral propagation of en echelon fault tips and formation of new connecting faults, possibly influenced by older northeast-striking structures (cf. Minor *et al.*, 2006). Short, transverse cross faults within the PFS, such as at Pajarito Canyon, are also likely to be associated with preexisting northeast-striking structural grain. The length of the fault system and, in part, its corrugated shape, may be controlled by the spacing of older structures.

The PFS has three principal bends, near Rendija Canyon, at St. Peter's Dome, and near Tent Rocks, that coincide with displacement deficits. The geometric complications posed by fault intersections at these bends may play important roles in strain accumulation and release, influencing rupture nucleation and propagation.

New paleoseismic data from a normal fault strand, interpreted in light of previous paleoseismic work, argue for three Holocene surface-rupturing earthquakes, one ca. 1.4 ka ago on the Pajarito fault, a second 6.5–5.2 ka ago on the Pajarito that is consistent with an event 6.5–4.2 ka ago on the Guaje Mountain fault, and a third ca. 9 ka ago on both the Pajarito and the Rendija Canyon faults. This paleoseismic event chronology demonstrates that the PF

sometimes ruptures alone, but at other times it ruptures along with the Rendija Canyon fault or the Guaje Mountain fault. When this occurs, the resultant seismic moment and therefore the earthquake magnitude are larger than when the main PF ruptures alone. The evidence for fault interaction suggests the potential for static stress concentrations and earthquake triggering. Given the evidence for youthful movement on the PFS, future ruptures that involve the main Pajarito and other faults of the PFS should be expected.

ACKNOWLEDGMENTS

This research was funded by the Offices of Nuclear Weapons Programs and Infrastructure, Facilities, and Construction at Los Alamos National Laboratory. We thank M. Machette, I. Wong, D. Koning, and A. Sussman for helpful discussions. Comments from C. Shaw, G. Smith, S. Minor, and an anonymous reviewer greatly improved this manuscript. This is Los Alamos National Laboratory publication LA-UR-06-2158.

REFERENCES CITED

- Aby, S.B., 1997, The terraces of Cochiti Canyon: Soil development and relation to tectonism in the Pajarito fault zone [M.S. thesis]: Albuquerque, University of New Mexico, 159 p.
- Aki, K., 1979, Characterization of barriers on an earthquake fault: *Journal of Geophysical Research*, v. 84, p. 6140–6148, doi: 10.1029/JB084iB11p06140.
- Baldrige, W.S., Keller, G.R., Haak, V., Wendlandt, E.D., Jiracek, G.R., and Olsen, K.H., 1995, The Rio Grande Rift, in Olsen, K.H., ed., *Continental rifts; evolution, structure, tectonics: Developments in Geotectonics Volume 25*: Amsterdam, Elsevier, p. 233–275.
- Boden, D.R., 1980, Stratigraphy of the Tshirege member of the Bandelier Tuff and structural analysis of the Pajarito fault zone, Bandelier National Monument Area, Jemez Mountains, New Mexico [M.S. thesis]: Golden, Colorado School of Mines, 187 p.
- Broxton, D.E., and Reneau, S.L., 1995, Stratigraphic nomenclature of the Bandelier Tuff for the Environmental Restoration Project at Los Alamos National Laboratory: Los Alamos National Laboratory Report LA-13010-MS, 21 p.
- Carey, W.J., and Cole, G., 2002, Description of the Cerro Grande fire laser altimetry (LIDAR) data set: Los Alamos National Laboratory Report LA-13892-MS, 57 p.
- Carter, K.E., and Gardner, J.N., 1996, Quaternary fault kinematics in the northwestern Espanola Basin, Rio Grande rift, New Mexico: *New Mexico Geological Society Guidebook*, v. 46, p. 97–103.
- Caskey, S.J., and Wesnousky, S.G., 1997, Static stress changes and earthquake triggering during the 1954 Fairview Peak and Dixie Valley earthquakes, central Nevada: *Seismological Society of America Bulletin*, v. 87, p. 521–527.
- Chapin, C.E., and Seager, W.R., 1975, Evolution of the Rio Grande rift in the Socorro and Las Cruces areas: *New Mexico Geological Society Guidebook*, v. 26, p. 297–321.
- Cowie, P.A., and Scholz, C.H., 1992, Displacement-length scaling relationship for faults: Data synthesis and discussion: *Journal of Structural Geology*, v. 14, p. 1149–1156, doi: 10.1016/0191-8141(92)90066-6.
- Crider, J.G., 2001, Oblique slip and the geometry of normal fault linkage: Mechanics and a case study from the Basin and Range in Oregon: *Journal of Structural Geology*, v. 23, p. 1997–2009, doi: 10.1016/S0191-8141(01)00047-5.
- Dawers, N.H., and Anders, M.H., 1995, Displacement-length scaling and fault linkage: *Journal of Structural Geology*, v. 17, p. 607–614, doi: 10.1016/0191-8141(94)00091-D.

- Dethier, D.P., 2003, Geologic map of the Puye quadrangle, Los Alamos, Rio Arriba, Sandoval, and Santa Fe Counties, New Mexico: U.S. Geological Survey Miscellaneous Field Studies Map MF-2419, scale 1:24,000.
- Dethier, D.P., and Reneau, S.L., 1995, Quaternary history of the western Española basin, New Mexico: *New Mexico Geological Society Guidebook*, v. 46, p. 289–298.
- Doser, D.I., 1985, Source parameters and faulting processes of the 1959 Hebgen Lake, Montana, earthquake sequence: *Journal of Geophysical Research*, v. 90, p. 4537–4555, doi: 10.1029/JB090iB06p04537.
- Doser, D., 1986, Earthquake processes in the Rainbow Mountain–Fairview Peak–Dixie Valley, Nevada region 1954–1959: *Journal of Geophysical Research*, v. 91, p. 12,572–12,586, doi: 10.1029/JB091iB12p12572.
- Ferrill, D.A., Stamatakos, J.A., and Sims, D., 1999, Normal fault corrugation: Implications for growth and seismicity of active normal faults: *Journal of Structural Geology*, v. 21, p. 1027–1038, doi: 10.1016/S0191-8141(99)00017-6.
- Gardner, J.N., and Goff, F., 1984, Potassium-argon dates from the Jemez volcanic field: Implications for tectonic activity in the north-central Rio Grande rift: *New Mexico Geological Society Guidebook*, v. 35, p. 75–81.
- Gardner, J.N., and House, L., 1987, Seismic hazards investigations at Los Alamos National Laboratory, 1984 to 1985: Los Alamos National Laboratory Report LA-11072-MS, 76 p.
- Gardner, J.N., Lavine, A., WoldeGabriel, G., Krier, D., Vaniman, D., Caporuscio, F., Lewis, C., Reneau, P., Kluk, E., and Snow, M., 1999, Structural geology of the northwestern portion of Los Alamos National Laboratory, Rio Grande rift, New Mexico: Implications for seismic surface rupture potential from TA-3 to TA-55: Los Alamos National Laboratory Report LA-13589-MS, 112 p.
- Gardner, J.N., Reneau, S.L., Lewis, C.J., Lavine, A., Krier, D.J., WoldeGabriel, G., and Guthrie, G.D., 2001, Geology of the Pajarito fault zone in the vicinity of S-Site (TA-16), Los Alamos National Laboratory, Rio Grande rift, New Mexico: Los Alamos National Laboratory Report LA-13831-MS, 86 p.
- Gardner, J.N., Reneau, S.L., Lavine, A., Lewis, C.J., Katzman, D., McDonald, E.V., Lepper, K., Kelson, K.L., and Wilson, C., 2003, Paleoseismic trenching in the Guaje Mountain fault zone, Pajarito fault system, Rio Grande rift, New Mexico: Los Alamos National Laboratory Report LA-14087-MS, 68 p.
- Goff, F., Gardner, J.N., and Valentine, G., 1990, Geology of St. Peter's Dome area, Jemez Mountains, New Mexico: *New Mexico Bureau of Mines and Mineral Resources Geologic Map 69*, scale 1:24,000.
- Goff, F., Gardner, J.N., and Reneau, S.L., 2001, Geology of the Frijoles 7.5-min. quadrangle, Los Alamos and Sandoval Counties, New Mexico: *New Mexico Bureau of Geology and Mineral Resources Open-File Geologic Map OF-GM 42*, scale 1:24,000.
- Golombek, M.P., 1981, Structural analysis of the Pajarito fault zone in the Espanola Basin of the Rio Grande rift, New Mexico [Ph.D. thesis]: Amherst, University of Massachusetts, 129 p.
- Gomberg, J., and Johnson, P.A., 2005, Dynamic triggering of earthquakes: *Nature*, v. 437, p. 830, doi: 10.1038/437830a.
- Griggs, R.L., 1964, Geology and ground water resources of the Los Alamos area, New Mexico: U.S. Geological Survey Water-Supply Paper 1753, 107 p.
- Hardy, S., and McClay, K., 1999, Kinematic modelling of extensional fault-propagation folding: *Journal of Structural Geology*, v. 21, p. 695–702, doi: 10.1016/S0191-8141(99)00072-3.
- Harrington, C.D., and Aldrich, M.J., 1984, Development and deformation of Quaternary surfaces on the northeastern flank of the Jemez Mountains: *New Mexico Geological Society Guidebook*, v. 35, p. 235–240.
- Izett, G.A., and Obradovich, J.D., 1994, ⁴⁰Ar/³⁹Ar age constraints for the Jaramillo Normal Subchron and the Matuyama-Brunhes geomagnetic boundary:

- Journal of Geophysical Research, v. 99, p. 2925–2934, doi: 10.1029/93JB03085.
- Jackson, J.A., 1982, Seismicity, normal faulting, and the geomorphological development of the Gulf of Corinth (Greece): The Corinth earthquakes of February and March 1981: *Earth and Planetary Science Letters*, v. 57, no. 2, p. 377–397.
- Kelley, V.C., 1979, Tectonics, middle Rio Grande rift, New Mexico, in Riecker, R.E., ed., *Rio Grande Rift: Tectonics and magmatism*: Washington, D.C., American Geophysical Union, p. 57–70.
- Kelson, K.I., Hemphill-Haley, M.A., Olig, S.S., Simpson, G.D., Gardner, J.N., Reneau, S.L., Kolbe, T.R., Forman, S.L., and Wong, I.G., 1996, Late-Pleistocene and possibly Holocene displacement along the Rendija Canyon fault, Los Alamos County, New Mexico: *New Mexico Geological Society Guidebook*, v. 47, p. 153–160.
- Kelson, K.I., Bauer, P.W., Unruh, J.R., and Bott, J.D.J., 2004, Late Quaternary characteristics of the northern Embudo fault, Taos County, New Mexico: *New Mexico Geological Society, 55th Field Conference, Guidebook*, p. 147–157.
- Kempton, K.A., and Kelley, S., 2002, *Geology of the Guaje Mountain 7.5-min. quadrangle, Los Alamos and Sandoval Counties, New Mexico*: New Mexico Bureau of Geology and Mineral Resources Open-File Geologic Map OF-GM 55, scale 1:24,000.
- Kite, W.M., 1985, Caldera-forming eruption sequences and facies variations in the Banderier Tuff, Central NM [M.S. thesis]: Tempe, Arizona State University, 376 p.
- Kleinfelder, Inc., 2005, Well R-26 completion report, Los Alamos National Laboratory: Albuquerque, New Mexico, unpublished consulting report prepared for the United States Department of Energy and the National Nuclear Security Administration, 33 pp.
- Koning, D.J., Aby, S.B., and Dunbar, N., 2004, Middle-upper Miocene stratigraphy of the Velarde graben, north-central New Mexico: Tectonic and paleogeographic implications: *New Mexico Geological Society Guidebook*, v. 55, p. 359–373.
- Koning, D., Skotnicki, S., Kelley, S., and Moore, J., 2005, *Geology of the Chili 7.5-min. quadrangle, Rio Arriba County, New Mexico*: New Mexico Bureau of Geology and Mineral Resources Open-File Geologic Map OF-GM 103, scale 1:24,000.
- Lavine, A., Lewis, C.J., Katcher, D.K., Gardner, J.N., and Wilson, J.E., 2003, *Geology of the north-central to northeastern portion of Los Alamos National Laboratory, New Mexico*: Los Alamos National Laboratory Report LA-14043-MS, 44 p.
- Lewis, C.J., Lavine, A., Reneau, S.L., Gardner, J.N., Channell, R., and Criswell, C.W., 2002, *Geology of the western part of Los Alamos National Laboratory (TA-3 to TA-16), Rio Grande rift: New Mexico*: Los Alamos National Laboratory Report LA-13960-MS, 98 p.
- Lynch, S.D., Smith, G.A., and Kuhle, A.J., 2004, *Geology of the Cañada 7.5-min. quadrangle, Sandoval County, New Mexico*: New Mexico Bureau of Mines and Mineral Resources Open-File Geologic Map OF-GM 85, scale 1:24,000.
- McCalpin, J.P., 1997, *Geomorphology and structure of the Pajarito fault zone west of Los Alamos National Laboratory, New Mexico*: Estes Park, Colorado, GEO-HAZ Consulting Inc., unpublished consulting report prepared for Los Alamos National Laboratory.
- McCalpin, J.P., 2005, Late Quaternary activity of the Pajarito fault, Rio Grande rift of northern New Mexico, USA: *Tectonophysics*, v. 408, p. 213–236, doi: 10.1016/j.tecto.2005.05.038.
- McDonald, E.V., Reneau, S.L., and Gardner, J.N., 1996, Soil-forming processes on the Pajarito Plateau: Investigation of a soil chronosequence in Rendija Canyon: *New Mexico Geological Society Guidebook*, v. 47, p. 367–382.
- Minor, S.A., Hudson, M.R., Grauch, V.J.S., and Sawyer, D.A., 2006, Structure of the Santo Domingo Basin and La Bajada constriction area, in Minor, S.A., ed., *The Cerrillos uplift, the La Bajada constriction, and hydrogeologic framework of the Santo Domingo Basin, Rio Grande rift, New Mexico*: U.S. Geological Survey Professional Paper 1720, p. 87–115.
- Nicol, A., Walsh, J.J., Waterson, J., and Underhill, J.R., 1997, Displacement rates of normal faults: *Nature*, v. 390, p. 157–159, doi:10.1038/36548.
- Olig, S., Kelson, K.I., Gardner, J.N., Reneau, S.L., and Hemphill-Haley, M., 1996, Earthquake potential of the Pajarito fault system, New Mexico: *New Mexico Geological Society Guidebook*, v. 47, p. 143–151.
- Peacock, D.C.P., and Sanderson, D.J., 1991, Displacements, segment linkage, and relay ramps in normal fault zones: *Journal of Structural Geology*, v. 13, p. 721–733, doi: 10.1016/0191-8141(91)90033-F.
- Peacock, D.C.P., and Sanderson, D.J., 1994, Geometry and development of relay ramps in normal fault systems: *American Association of Petroleum Geologists Bulletin*, v. 78, p. 147–165.
- Phillips, E.H., 2004, Collapse and resurgence of the Valles caldera, Jemez Mountains, New Mexico: ⁴⁰Ar/³⁹Ar age constraints on the timing and duration of resurgence and ages of megabreccia blocks [M.S. thesis]: Socorro, New Mexico Institute of Mining and Technology, 200 p.
- Reilinger, R.E., and York, J.E., 1979, Relative crustal subsidence from leveling data in a seismically active part of the Rio Grande Rift, New Mexico: *Geology*, v. 7, p. 139–143, doi:10.1130/0091-7613(1979)7<139:RCSFLD>2.0.CO;2.
- Reimer, P.J., and 27 others, 2004, IntCal04 terrestrial radiocarbon age calibration, 0–26 cal kyr BP: *Radiocarbon*, v. 46, p. 1029–1058.
- Reneau, S.L., 2000, Stream incision and terrace development in Frijoles Canyon, Banderier National Monument, New Mexico, and the influence of lithology and climate: *Geomorphology*, v. 32, p. 171–193, doi:10.1016/S0169-555X(99)00094-X.
- Reneau, S.L., Gardner, J.N., Lavine, A., McDonald, E.V., Lewis, C., Katzman, D., WoldeGabriel, G., Krier, D., Bergfeld, D., and Heikoop, J., 2002, Paleoseismic investigation of Trench EOC-2, Pajarito fault zone, Los Alamos National Laboratory, New Mexico: Los Alamos National Laboratory Report LA-13939-MS, 65 p.
- Scholz, C.H., 1982, Scaling laws for large earthquakes: Consequences of physical models: *Seismological Society of America Bulletin*, v. 72, p. 1–14.
- Scholz, C.H., and Gupta, A., 2000, Fault interactions and seismic hazard: *Journal of Geodynamics*, v. 29, p. 459–467, doi: 10.1016/S0264-3707(99)00040-X.
- Self, S., Goff, F., Gardner, J.N., Wright, J.V., and Kite, W.M., 1986, Explosive rhyolitic volcanism in the Jemez Mountains: Vent locations, caldera development and relation to regional structure: *Jour. Geophys. Res.*, v. 91, no. B2, p. 1779–1798.
- Smith, G.A., and Kuhle, A.J., 1998, *Geology of the Santo Domingo Pueblo and Santo Domingo SW 7.5' quadrangles, Sandoval County, New Mexico*: New Mexico Bureau of Mines and Mineral Resources Open-File Geologic Map OF-GM 15 and 26, scale 1:24,000.
- Smith, G.A., McIntosh, W., and Kuhle, A.J., 2001, Sedimentologic and geomorphic evidence for seesaw subsidence of the Santo Domingo accommodation-zone basin, Rio Grande rift, New Mexico: *Geological Society of America Bulletin*, v. 113, p. 561–574, doi: 10.1130/0016-7606(2001)113<0561:SAGEFS>2.0.CO;2.
- Smith, R.L., 1960, Ash-flow tuffs: Their origin, geologic relations, and identification: U.S. Geological Survey Professional Paper 366, 81 p.
- Smith, R.L., Bailey, R.A., and Ross, C.S., 1970, *Geologic map of the Jemez Mountains, New Mexico*: U.S. Geological Survey Miscellaneous Investigations Map I-571, scale 1:125,000.
- Susong, D.D., Janecke, S.U., and Bruhn, R.L., 1990, Structure of a fault segment boundary in the Lost River fault zone, Idaho, and possible effect on the 1983 Borah Peak earthquake rupture: *Seismological Society of America Bulletin*, v. 80, p. 57–68.
- Tavarnelli, E., and Pasqui, V., 2000, Fault growth by segment linkage in seismically active settings: Examples from the Southern Apennines, Italy, and the Coast Ranges, California: *Journal of Geodynamics*, v. 29, p. 501–516, doi: 10.1016/S0264-3707(99)00041-1.
- Trudgill, B., and Cartwright, J., 1994, Relay-ramp forms and normal-fault linkages, Canyonlands National Park, Utah: *Geological Society of America Bulletin*, v. 106, p. 1143–1157, doi: 10.1130/0016-7606(1994)106<1143:RRFANF>2.3.CO;2.
- Vita-Finzi, C., and King, G.C.P., 1985, The seismicity, geomorphology and structural evolution of the Corinth area of Greece: *Royal Society of London Philosophical Transactions*, ser. A, v. 314, p. 379–407, doi: 10.1098/rsta.1985.0024.
- Wells, D.L., and Coppersmith, K.J., 1994, New empirical relationships among magnitude, rupture length, rupture width, rupture area, and surface displacement: *Seismological Society of America Bulletin*, v. 84, p. 974–1002.
- Westaway, R., Gawthorpe, R., and Tozzi, M., 1989, Seismological and field observations of the 1984 Lazio-Abruzzo earthquakes: Implications for the active tectonics of Italy: *Geophysical Journal*, v. 98, p. 489–514, doi: 10.1111/j.1365-246X.1989.tb02285.x.
- Willsey, S.P., Umhoefer, P.J., and Hilley, G.E., 2002, Early evolution of an extensional monocline by a propagating normal fault: 3D analysis from combined field study and numerical modeling: *Journal of Structural Geology*, v. 24, p. 651–669, doi: 10.1016/S0191-8141(01)00120-1.
- Withjack, M.O., and Callaway, S., 2000, Active normal faulting beneath a salt layer: An experimental study of deformation patterns in the cover sequence: *American Association of Petroleum Geologists Bulletin*, v. 84, p. 627–651.
- Withjack, M.O., Olson, J., and Peterson, E., 1990, Experimental models of extensional forced folds: *American Association of Petroleum Geologists Bulletin*, v. 74, p. 1038–1054.
- WoldeGabriel, G., Warren, R.G., Cole, G., Goff, F., Broxton, D., Vaniman, D., Peters, L., and Naranjo, A., 2003, Periodicity and distribution of volcanism in the Pajarito Plateau, Rio Grande rift, north-central New Mexico: U.S. Geological Survey Open-File Report OF 03–0369, 7 p.
- Wong, I., Kelson, K., Olig, S., Kolbe, T., Hemphill-Haley, M., Bott, J., Green, R., Kanakari, H., Sawyer, J., Silva, W., Stark, C., Haraden, C., Fenton, C., Unruh, J., Gardner, J., Reneau, S., and House, L., 1995, *Seismic hazards evaluation of the Los Alamos National Laboratory*: Oakland, California, Woodward-Clyde Federal Services, unpublished consulting report prepared for Los Alamos National Laboratory, 3 volumes.
- Wong, I., Silva, W., Olig, S., Dover, M., Gregor, N., Gardner, J., Lewis, C., Terra, F., Zachariasen, J., Stokoe, K., Thomas, P., and Upadhyaya, S., 2007, Update of the probabilistic seismic hazard analysis and development of seismic design ground motions at the Los Alamos National Laboratory: Oakland, California, URS Corporation, unpublished consulting report prepared for Los Alamos National Laboratory, 1 volume.
- Zoback, M.L., Anderson, R.E., and Thompson, G.A., 1981, Cainozoic evolution of the state of stress and style of tectonics of the Basin and Range Province of the western United States: *Royal Society of London Philosophical Transactions*, ser. A, v. 300, p. 407–434, doi: 10.1098/rsta.1981.0073.

MANUSCRIPT RECEIVED 11 JULY 2008

REVISED MANUSCRIPT RECEIVED 12 JANUARY 2009

MANUSCRIPT ACCEPTED 13 FEBRUARY 2009